Shell Beds in Ordovician storm- to tide-dominated deposits, Daoura (Ougarta range), Algeria

Imene Metatla, Jean-Yves Reynaud, Jean-François Ghienne, Olev Vinn, Chakib Harouz, Abderrazak El Albani, Arnaud Mazurier & Salamet Mahboubi

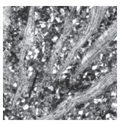

The Ordovician wave-dominated sandstones of the Daoura (Ougarta range, NW Algeria) contain shell beds with cornulitids in an exceptional state of preservation. The objective of this study, focused on the sandstone of the uppermost part of the Hassi Chaamba Fm. (Sandbian?), is to understand the shell beds from the hydrodynamic and stratigraphic perspective with the combined approach of facies sedimentology and taphonomy. A 40-m section encompassing the shell beds was studied in detail. The shell beds are preserved as dm-scale concentrations in transgressive deposits of 5 high-frequency sequences preserved at the turnaround from a regressive to a transgressive sequence set. The biota in shell beds are dominated by brachiopods, cornulitids and gastropods, suggesting that the related ecosystem extended to the offshore. Three types of shell beds are distinguished, ranging from a conglomerate in the foreshore to a hardground in the offshore transition. In the lower shoreface, the shell beds are interstratified with fine-sand SCS infilling large-scale (up to 20 m in wavelength) troughs eroded in the foreshore by transgressive ravinement. The petrographic and tomographic analysis of a sample of these shell beds shows that cornulitids and, to a lesser extent, brachiopods of the shell beds are perfectly preserved within a matrix composed of bioclasts. This suggests that they were reworked from nearby areas and therefore were present in the foreshore. Aggregation of cornulitids in clusters of 4–5 individuals suggests an adaptation to loose grounds in a relatively high energy setting. The rhythmic alternation of shell beds and sandstones in these deposits suggests a possible role of tides in their formation. • Key words: Upper Ordovician, wave-dominated ramp, shell beds, tide-modulated shoreface, cornulitids, tempestites, Daoura, Ougarta, Algeria.

Metatla, I., Reynaud, J.-Y., Ghienne, J.-F., Vinn, O., Harouz, C., El Albani, A., Mazurier, A. & Mahboubi, S. 2024. Shell Beds in Ordovician storm- to tide-dominated deposits, Daoura (Ougarta range), Algeria. *Bulletin of Geosciences 99*(*2*), 149–168 (11 figures). Czech Geological Survey, Prague. ISSN 1214-1119. Manuscript received October 27, 2023; accepted in revised form April 26, 2024; published online May 19, 2024; issued June 2, 2024.

Imene Metatla, Laboratoire d'Océanologie et Géosciences (LOG UMR 8187CNRS), Université de Lille, Université du Littoral Côte d'Opale, Institut de Recherche et de Développement, Cité Scientifique, F-59655 Villeneuve d'Ascq, Lille, France & Laboratoire de géodynamique des bassins sédimentaires et des orogènes, département de Géologie, Faculté des Sciences de la Terre, Géographie et de l'Aménagement de Territoire, Université des Sciences et de la Technologie Houari Boumediene, Bab Ezzouar, Alger, Algérie • Jean-Yves Reynaud, Laboratoire d'Océanologie et Géosciences (LOG UMR 8187CNRS), Université de Lille, Université du Littoral Côte d'Opale, Institut de Recherche et de Développement, Cité Scientifique, F-59655 Villeneuve d'Ascq, Lille, France; jean-yves.reynaud@univ-lille.fr • Jean-François Ghienne, Institut Terre et Environnement de Strasbourg, UMR7063, 5 rue R. Descartes, F-67000 Strasbourg, France • Olev Vinn, Department of Geology, University of Tartu, Ravila 14 A, 50411 Tartu, Estonia • Chakib Harouz, Laboratoire de géodynamique, géologie de l'ingénieur et de planétologie, Faculté des Sciences de la Terre, Géographie et de l'Aménagement de Territoire, Université des Sciences et de la Technologie Houari Boumediene, Bab Ezzouar, Alger, Algérie • Abderrazak El Albani & Arnaud Mazurier, IC2MP, UMR 7285, CNRS, Université de Poitiers, France • Salamet Mahboubi, Université de Tlemcen, Laboratoire de Recherche n°25 Tlemcen, Algérie

Cambro–Ordovician deposits covering wide epicratonic platforms around the western Gondwana constitute one of the major, highly mature clastic wedges from the geological record (Fabre 1988; Avigad *et al*. 2005; Sabaou *et al*. 2009; Altumi *et al*. 2013; Bassis *et al*. 2016; Ghienne *et al*. 2010, 2023; Elicki *et al*. 2023). This context and the resulting stratal organization display non-actualistic features such as: (i) the absence of clearly defined large-scale clinoform systems (Ghienne *et al*. 2007), which would highlight continental-scale deltaic fairways; (ii) low but continuous, and then finally significant subsidence rate in basinal areas (Perron *et al*. 2018); (iii) a lack of incised-valley systems and related estuarine fills despite recurrent and significant sea-level fluctuations (Loi *et al*. 2010) and tidal influence (Poiré *et al*. 2003, Gil-Ortiz *et al*. 2019, 2022); (iv) thick (50–500 m) storm-dominated,

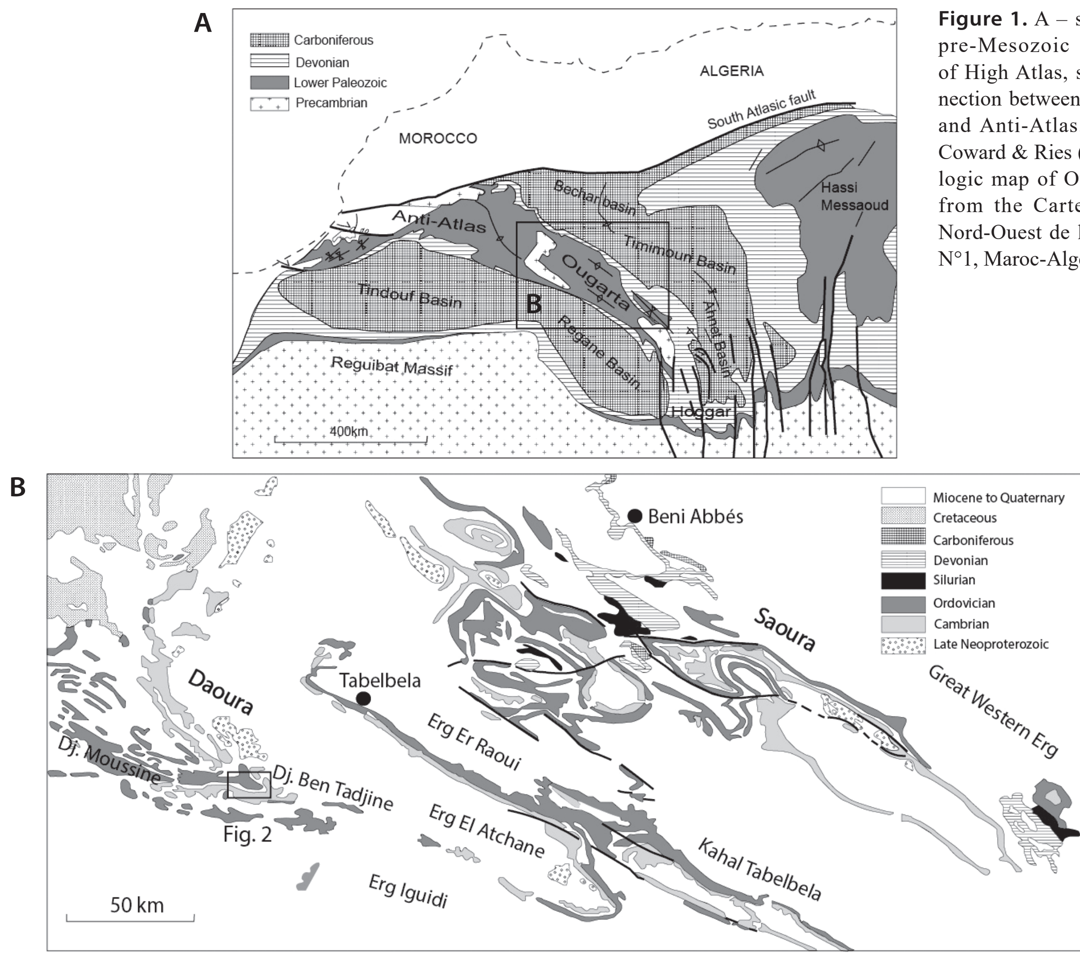

Figure 1. A – structural map of pre-Mesozoic basement south of High Atlas, showing the connection between Hoggar, Ougarta and Anti-Atlas. Modified from Coward & Ries (2003). • B – geologic map of Ougarta. Modified from the Carte géologique du Nord-Ouest de l'Afrique, Feuille N°1, Maroc-Algérie Ouest 1952.

coarsening- and thickening-upward regressive successions alternating with 5–50 m thick, tide-dominated sandstone units interpreted as transgressive and localized in specific paleogeographic areas of the basin (Ghienne *et al*. 2007, 2023; Marante 2008). Overall, it results a shale–sandstone partitioning marked on second-order (5–15 Ma) stratigraphic cycles and long-range extent (> 1000 km) of the corresponding units of the lithostratigraphy. In an essentially pre-vegetation context (Davies & Gibling 2010), a protracted high-rate of sediment supply over the platform might explain some of these features by extending the width of the fluvial–shallow-marine transition zone (Shchepetkina *et al*. 2019) and bypassing fine-grained sediments toward the outer shelf.

In this context, more indications for distributed tidal processes might be expected throughout the depositional record. Tidal influence or modulation have been recently emphasized from storm- to wave-dominated depositional systems (Dashtgard *et al*. 2012, Vakarelov *et al*. 2012, Vaucher *et al*. 2017, Jelby *et al*. 2020). In this paper, we aim to decipher the potential tidal signature from an Ordovician, storm-dominated sequence from the Daoura range (Ougarta Mountains, NW Algeria). Here, shell concentrations were investigated in detail, documenting the geometry of beds and laminae (field observation and microtomography X), the stacking pattern of the related succession, and the faunal content that includes rare examples of well-preserved cornulitids (*e.g.*, Gutiérrez-Marco & Vinn 2018). Similar shell beds recurrently formed in the Ordovician successions of Algeria and Morocco (Álvaro *et al*. 2007 a, b; Ghienne *et al*. 2007; Loi *et al*. 2010; Vaucher *et al*. 2016; Popov *et al*. 2019). Various types of concentrations have been described and interpreted in relation with sea-level fluctuations linked to either tidal (Vaucher *et al*. 2016) or high-frequency, mostly orbitally-controlled cycles, with which storm events interfere (Botquelen *et al*. 2004, Loi *et al*. 2010, Colmenar & Álvaro 2015, Álvaro *et al*. 2022). However, the bed fabric and taphonomy of those facies have never been used to detect the interplay of processes controlling their formation and preservation. An exceptional outcrop of Djebel Moussine allows to reconsider the possible interplay of tides in these shell beds. We also use these data to illustrate how cornulitids can be used to infer hydrodynamic patterns from the depositional record.

Geological setting

The Ougarta Mountains correspond to a metacratonic domain, where a Variscan deformation zone, extending over 300 km, has reactivated the ancient margin of the West African Craton (Fig. 1A) (Ziegler *et al.* 1995, Ennih & Liégeois 2001, Brahimi *et al*. 2018, Melouah *et al.* 2021). Related Variscan folds, oriented NW–SE, connect to those of the eastern Anti-Atlas in southern Morocco (Donzeau *et al*. 1981, Lamali *et al*. 2013, Baidder *et al*. 2016, Michard *et al.* 2023) and have been truncated and unconformably onlapped by Meso–Cenozoic sediments of the Saharan platform (Busson 1972, Askri *et al*. 1995). The Ougarta Moutains expose a thick (> 3000 m) Paleozoic succession that was deposited over the 'North-Gondwana' platform, and which appears as the southeastward extension of the Anti-Atlas outcrops (Ait Kaci 1990, Fabre & Kazi-Tani 2005, Ghienne *et al*. 2007). This succession exposes a stratigraphic record that is otherwise essentially present in the subsurface in the adjacent Algerian North-Saharan basins (Tindouf, Regane, Bechar, Timimoun, Ahnet Basin) (Fig. 1A; Askri *et al.* 1995, Nedjari & Ait Ouali 2006, Craig *et al*. 2009, Eschard *et al.* 2010, Galeazzi *et al*. 2010, Perron *et al*. 2018, Ghienne *et al.* 2023).

Two parallel mountain ranges separated by the Er Raoui sand sea (Erg er Raoui) are distinguished in the Ougarta Mountains: the Saoura range to the NE, and the Daoura range to the SW, the latter including the Kahal Tabelbela and the Djebel Ben Tadjine-Djebel Moussine mountains; the latter including our study area (Fig. 1B). The Saoura range was instrumental in establishing the regional, Lower Paleozoic stratigraphy (Menchikoff 1930; Pouyeto 1952; Gomes Silva *et al.* 1963; Legrand 1966, 1974, 1985). Its Ordovician stratigraphy and related faunal record have also been the target of the more recent studies (Hamdidouche 2009, Makhlouf *et al.* 2018, Popov *et al.* 2019, Legrand & Bouterfa 2021, Naimi *et al.* 2023). By contrast, the Daoura range is still poorly explored and the stratigraphic framework dates back from the oil exploration years (BEICIP 1972, Gomez Silva *et al.* 1963, Ait Kaci 1990). The only recent study concerns the igneous basement (Mekkaoui *et al*. 2017). However, the Daoura stratigraphy preserves a thick and relatively continuous Cambrian to Ordovician record above the "infra-Tassilian" unconformity (Fig. 2; Chikhaoui & Donzeau 1972, Fabre 1988).

In both the Saoura and Daoura ranges, Cambrian clastics correspond mostly to braided fluvial systems. The upper part of the Cambrian sandstones shows the transition to a marine sedimentation and the Cambrian–Ordovician boundary is positioned to a lingulid shell bed ("dalle à lingules"). Ordovician strata consist of an alternation of offshore fine-grained deposits and

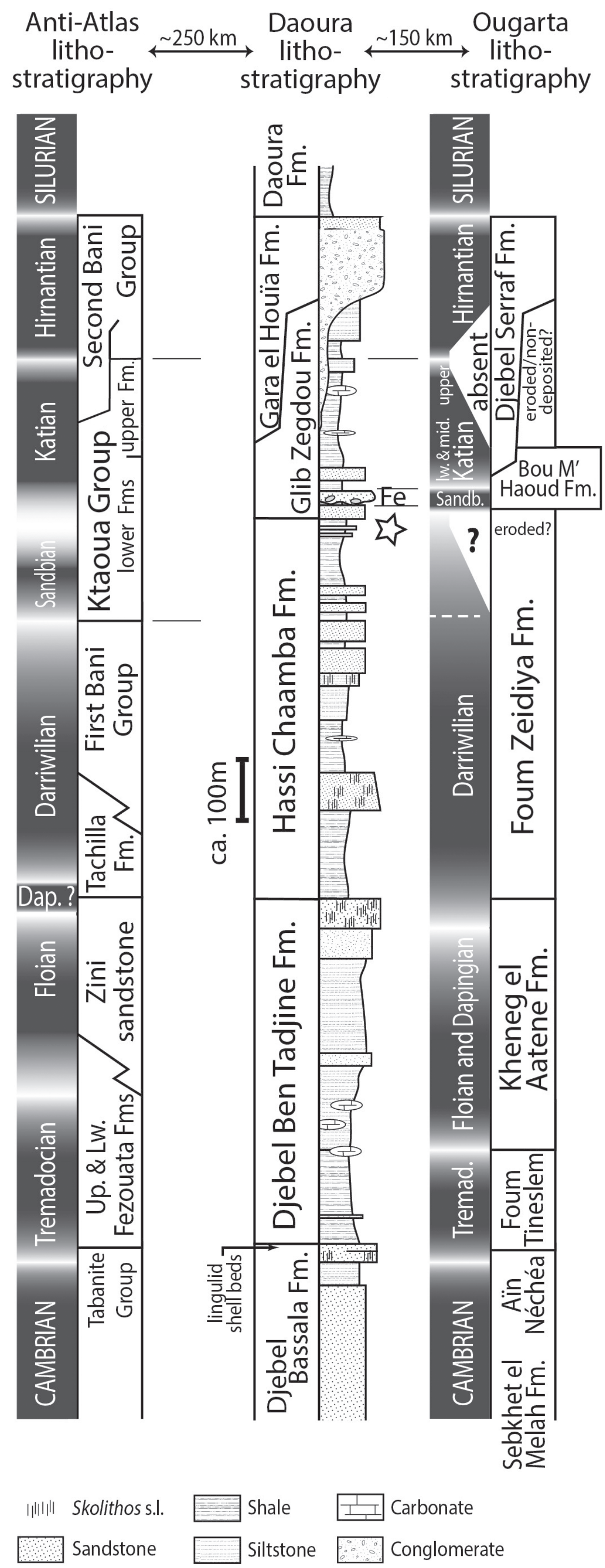

Figure 2. Lithostratigraphic column of Ordovician formations of Daoura and proposed correlations with Ougarta (Saoura range) and Anti-Atlas. See text for explanations. The star indicates the location of shell beds.

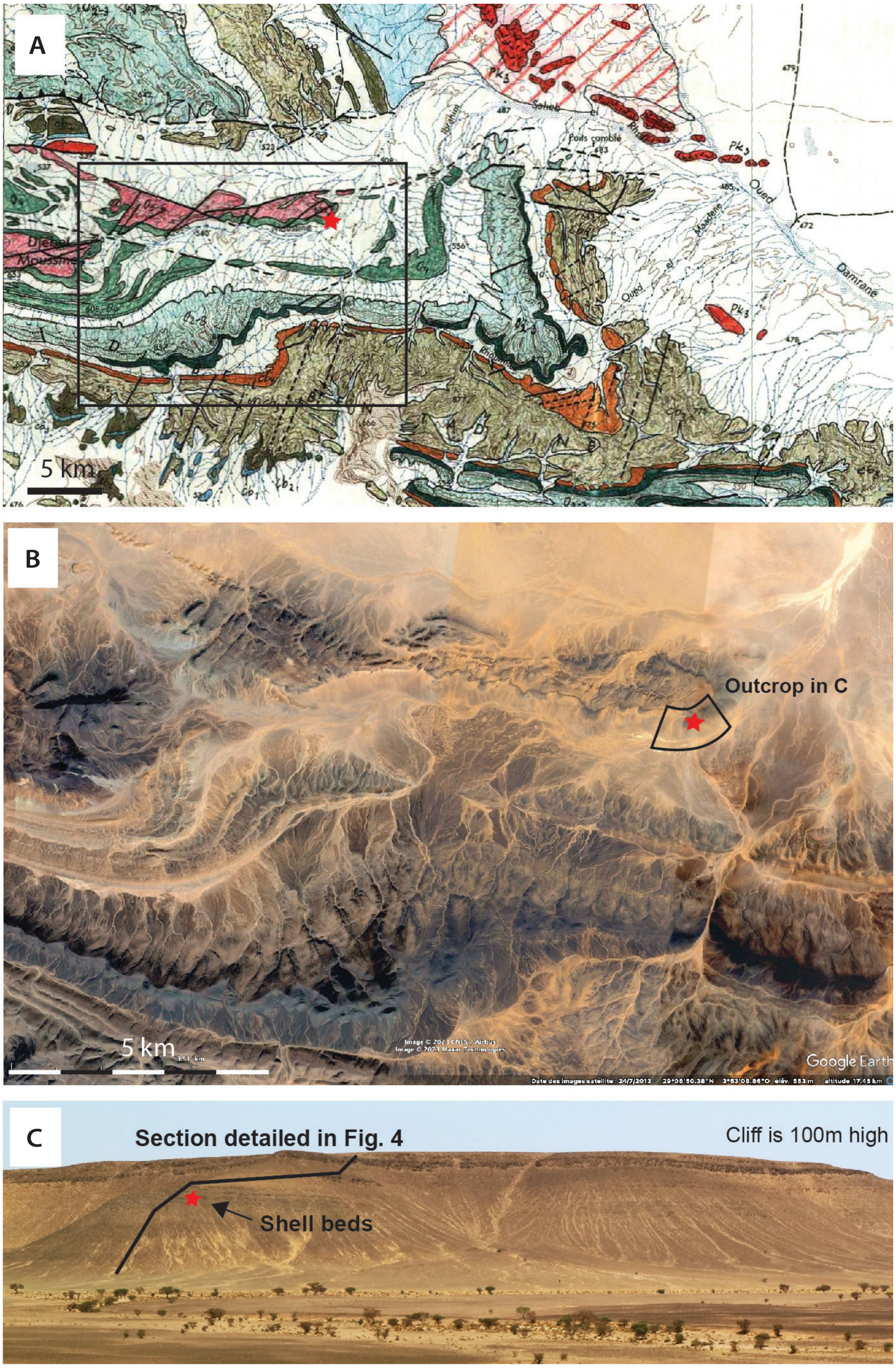

Figure 3. A – original map of BEICIP (1972) with stratigraphic units derived from the Saoura range (see Fig. 2). The red star indicates the location of the shell beds. • B – satellite image of the frame in A, showing the location of studied section. • C – location of the studied section. The shell beds coordinates are 29° 8′ 4.24″ N, 3° 50′ 2.29″ W.

shallow-marine sandstones (storm- and tide-dominated depositional environments; Ghienne *et al*. 2007, Hamdidouche 2009, Legrand & Bouterfa 2021), which constitute a more proximal sedimentary record relative to that of the Moroccan Anti-Atlas (Table 1; Destombes 1985; Álvaro *et al*. 2007a, b, 2022; Marante 2008; Loi *et al*. 2010; Ghienne *et al*. 2014; Meddour 2016; Vaucher *et al*. 2017). As in other parts of NW Africa, the Ordovician record ends with the unconformable deposits of the Hirnantian glaciation (Ghienne *et al*. 2023). In the Saoura, the younger pre-glaciation deposits are attributed to the middle Katian (Popov *et al*. 2019). The Ordovician succession in the Daoura is more complete than that of the Saoura range; Late Katian to pre-glaciation Hirnantian

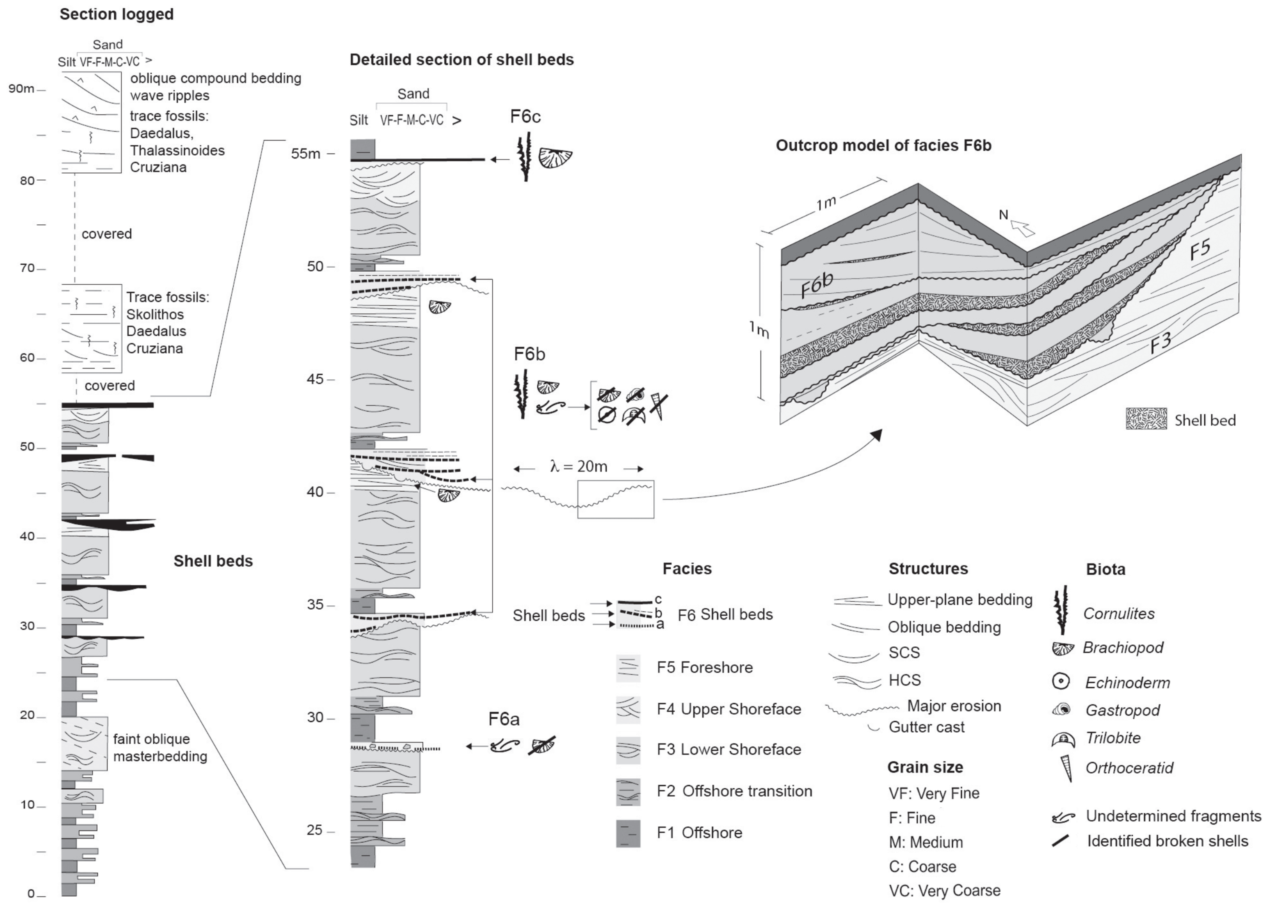

Figure 4. Section logged – complete section as located in Fig. 3C; the upper part, with numerous trace fossils and no wave dynamics, is not discussed in this paper. Detailed section of shell beds. Outcrop model of facies F6b – shell bed featured in Fig. 6A.

deposits were identified there (from Destombes 1983, in Ghienne *et al*. 2023). Silurian–Devonian shales, sandstones and limestones are largely developed in the Saoura range (Boumendjel *et al*. 1997, Legrand 2003, Mehadji *et al.* 2011), but only Silurian remnants are known in the Daoura range.

The Daoura range offers exceptional conditions for investigating the Cambro–Ordovician strata, which crop out as cuestas in a desert landscape. Cliff-forming sandstone units are usually traceable for tens of kilometers but shale-dominated intervals are largely covered by Quaternary wadis deposits. Ordovician strata of the Daoura have been subdivided into four formations, from base to top (BEICIP 1972): Djebel Ben Tadjine Fm., Hassi Chaamba Fm., Glib Zegdou Fm. and Gara el Houïa Fm. Those formations essentially correspond to Lower Ordovician, Middle Ordovician (and lowermost Upper Ordovician?), Upper Ordovician, and uppermost ('upper' Hirnantian) units, respectively (Fig. 2).

In this article, we focus on sandstones of the uppermost Hassi Chaamba Formation, which are distinct by the occurrence of shell beds (Fig. 3A). Similar shell beds were also reported from correlatable horizons of the Saoura range (upper part Foum ez Zeidiya Fm.; Ghienne *et al.* 2007, Popov *et al.* 2019, Legrand & Bouterfa 2021), but the age remains questionable. If the base of the Bou M'Haoud Fm. is placed at the base of a conglomeratic ferruginous marker bed, the lithologic correlation with the more proximal Ougarta sections suggests a Late Darriwilian age for the shell beds of the Daoura succession (Fig. 2). This possibility is in an agreement with the stratigraphic scheme of Ghienne *et al.* (2007) and Popov *et al*. (2019) who propose that the uppermost beds of the Foum Zeidiya Fm., devoid of fauna, can be attributed to the Darriwilian. However, comparison of the Daoura succession with the more distal Anti-Atlas succession (Fig. 2, left column) suggests a potential correlation with the Lower Ktaoua Group. Such a correlation would result in a Sandbian to Lower Katian age for the study interval. The contradiction can be resolved by considering the uppermost deposits of the Hassi Chaamba Fm. as Sandbian in age in the Daoura succession, and the Hassi Chaamba and Foum Zeidiya

Formations as not, strictly speaking, correlatable (Fig. 2). Occurrence of dalmanelloid brachiopods (*Tafilaltia*?) and of a rafinesquinid strophomenide (L. Popov, pers. comm.) associated with the studied shell beds would also favor an Upper Ordovician age (Colmenar *et al.* 2022).

Materials and methods

The sandstones and shell beds of the Hassi Chaamba Fm. examined in the study are exposed in the middle part of a 90 m high cuesta (Fig. 3C). The section (Fig. 4) was logged in detail using a Jacob staff (ASC Scientific) and sampling places were positioned with a GPS. About 50 kg of samples of shell beds were collected. Thin sections were studied using a BX60 polarizing microscope, equipped with a Spot Flex camera (Diagnostic Instrument) controlled by Spot Advanced software. Observations were also made with the SEM (FEI Quanta 200 equipped with an EDS probe). These analyzes were carried out at the LOG laboratory at the University of Lille. In addition, a microtomography analysis of a 400 cm^3 sample was carried out at the IC2MP laboratory (University of Poitiers) using RX-solutions EasyTom XL Duo equipment, equipped with a microfocus X-ray source and a nanofocus source (LaB6 filament) Hamamatsu, coupled with a Varian PaxScan 2520DX flat panel. The reconstructions were carried out using the XAct software (RX-solutions) using a classic filtered back-projection algorithm, with reduction of artifacts due to selective absorption of the beam. Virtual cuts, 3D renderings and videos were made with Avizo Fire V.9.2 (FEI).

Siliciclastic facies embedding the shell beds

Wave-dominated offshore transition

Description. – Facies F1 is composed of greenish to reddish shale (siltstone) that breaks into mm to cm plates. Facies F1 is supposed to constitute most of the shale intervals, several tens of meters thick, forming the lows between the cuestas and generally covered by Quaternary alluvial/colluvial facies or scree deposits from the hillslope (Fig. 3C). Facies F2, commonly interstratified with facies F1, is composed of decimeter-thick packages of laminated siltstone alternating with centimeter-scale beds of very fine sandstone, the latter including subdued hummocky cross-stratifications (HCS), a few cm in amplitude (Fig. 5A). This facies comprises a few horizontal burrows of *Cruziana* isp.

Interpretation. – The subdued bedforms and fine grain size of the F1–F2 facies indicate a dominant fallout process within a low energy distal environment. The small HCS indicate wave processes that can be linked to distal storms, below the fair-weather wave action limit (Harms *et al*. 1975, Jelby *et al*. 2020). Consequently, facies F2 is interpreted as an upper offshore (offshore transition) facies and facies F1, when found alone in meter-scale successions, would correspond to lower offshore deposits.

Wave-dominated shoreface to foreshore

Description. – Facies F3 consists of dm to meter-thick, fine- to medium-grained sandstone beds with pervasive HCS, a few dm in wavelength and a few cm in amplitude, systematically grading upward from facies F2 (Fig. 5A). The beds generally form upward-thickening successions (bedsets) up to 2 m in thickness, in which a gradual increase in the size of the HCS is observed. These bedsets are locally bounded by discontinuous, centimeter-scale mud drapes. Above the second occurrence of shell beds (36 m height in Fig. 4), the bedform wavelength increases so that parallel, subhorizontal lamination is commonly observed in place of the typical hummocks or swales and their associated erosional surfaces. Facies F4 overlies facies F3. It is composed of meters-thick sets of HCS and swaley cross-stratified (SCS) sandstone beds (Fig. 5B). These bedforms are up to 1.5 meter in wavelength and 40 cm in amplitude, often amalgamated but sometimes separated by mud drapes. Locally, a faint low-angle master bedding can be inferred despite amalgamation (Fig. 4). The uppermost occurrence of facies F4 shows a combination of SCS and upper-plane bedding, the two passing laterally to each other in the continuity of laminae (Fig. 6C). Facies F5 overlies either facies F3 or facies F4, by way of a faint erosion surface. It is composed by decimeter-scale layers of fine and well sorted sandstone, presenting planar and very low angle bedding (Fig. 6A). It contains sparse entire brachiopod shells along with brachiopod clusters (Fig. 6B).

Interpretation. – The HCS and SCS of facies F3 and F4 are interpreted as results of 3D oscillatory currents that classically occur in the shoreface during storm events (Cheel & Leckie 1993). The SCS reflects a lesser aggradation rate, related to a more erosional, proximal part of the shoreface profile (Dumas & Arnott 2006). The minor proportion of mud drapes suggests that the environment is subject to wave processes almost constantly, or that inter-storm deposits are entirely reworked. The SCS in F4 point to the upper shoreface, while the HCS with mud drapes in F3 relates to the lower shoreface (Harms *et al.* 1975, Brenchley *et al.* 1986, Jelby *et al*. 2020). The continuity of SCS and upper-plane bedding in facies F4 was noted earlier as a feature of the surf zone (Clifton *et al*. 1971).

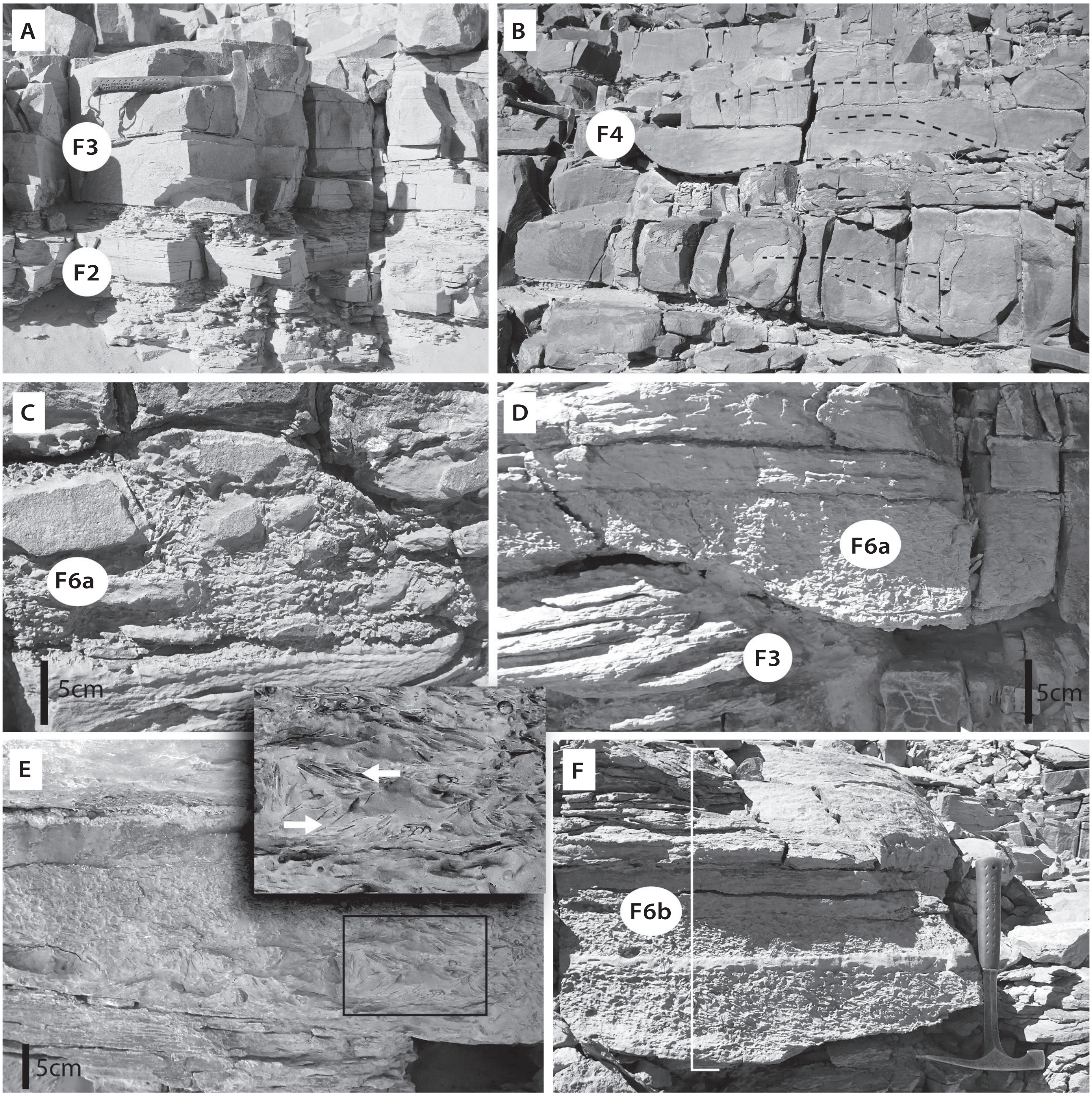

Figure 5. Facies on the logged section. • A – transition from offshore transition (F2) to shoreface (F3); 9 m. • B – succession of amalgamated HCS/SCS in the foreshore (F4); 15 m. Hammer for scale. • C – conglomerate in the first shell bed occurrence (F6a); 29 m. • D – this bed shows locally prominent basal erosion with scouring of the underlying shoreface (F3). • E – detail of the fabric of this shell bed. The white arrows indicate alternating layers with opposite imbrication. See text for details. • F – second shell bed occurrence (F6b), with a thin intervening sandstone layer; 34 m. The upper layer of sandstone forms a flat top abruptly overlain by facies F1 (covered by fallen blocks in the background of the picture).

Pervasive planar bedding and very low angle truncations of facies F5 are associated with supercritical flows in the swash or breaker zone and are therefore assigned to the foreshore (Clifton 1976). Occurrences where facies F5 sits directly above F3, without the intervening F4 (Fig. 4), suggest an abrupt increase in the size of the waves and/or decrease in water depth.

Shell beds

The term "shell bed" points to accumulations of shell debris or entire organisms (Kidwell *et al.* 1986, Botquelen *et al.* 2004, Álvaro *et al*. 2007a, b). The shell beds discussed in this article are grouped under three subfacies: F6a, F6b, F6c.

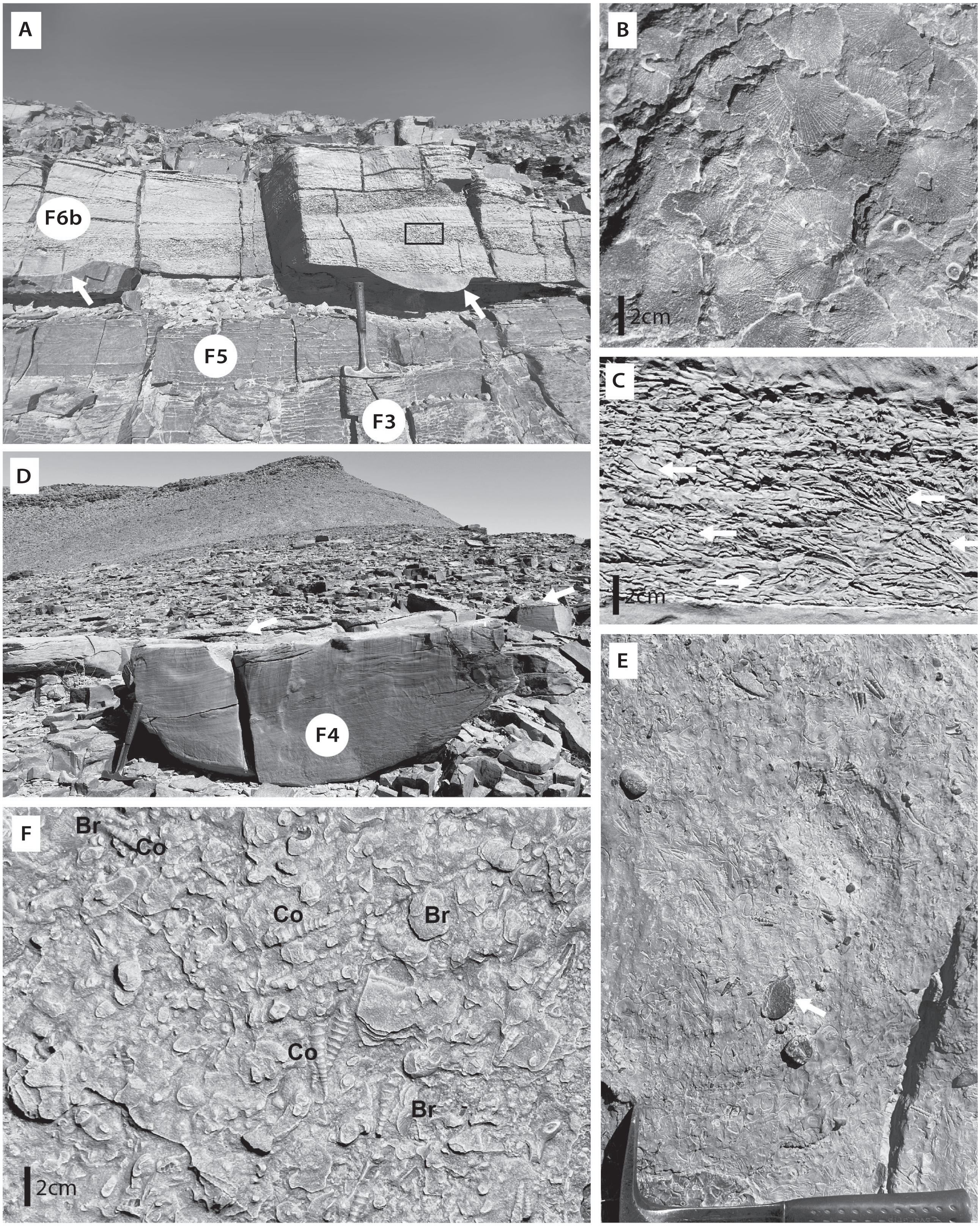

Figure 6. A – third shell bed occurrence at 41 m. White arrows point to gutter casts. The shell beds are interstratified with sandstones, a typical feature of this facies (F6b). Note the upper-plane bedding in the underlying sandstone (F5). • B – cluster of brachiopods found in facies F5 in picture A. • C – detail of shell bed fabric corresponding to black frame in Fig. 6A. It shows the same rhythmic stratification as in facies F6a (Fig. 5E), with 2-cm thick intervals of oblique, imbricated flat bioclasts of brachiopods or entire cornulitids bounded by veneers of flat bioclasts. Imbrications show

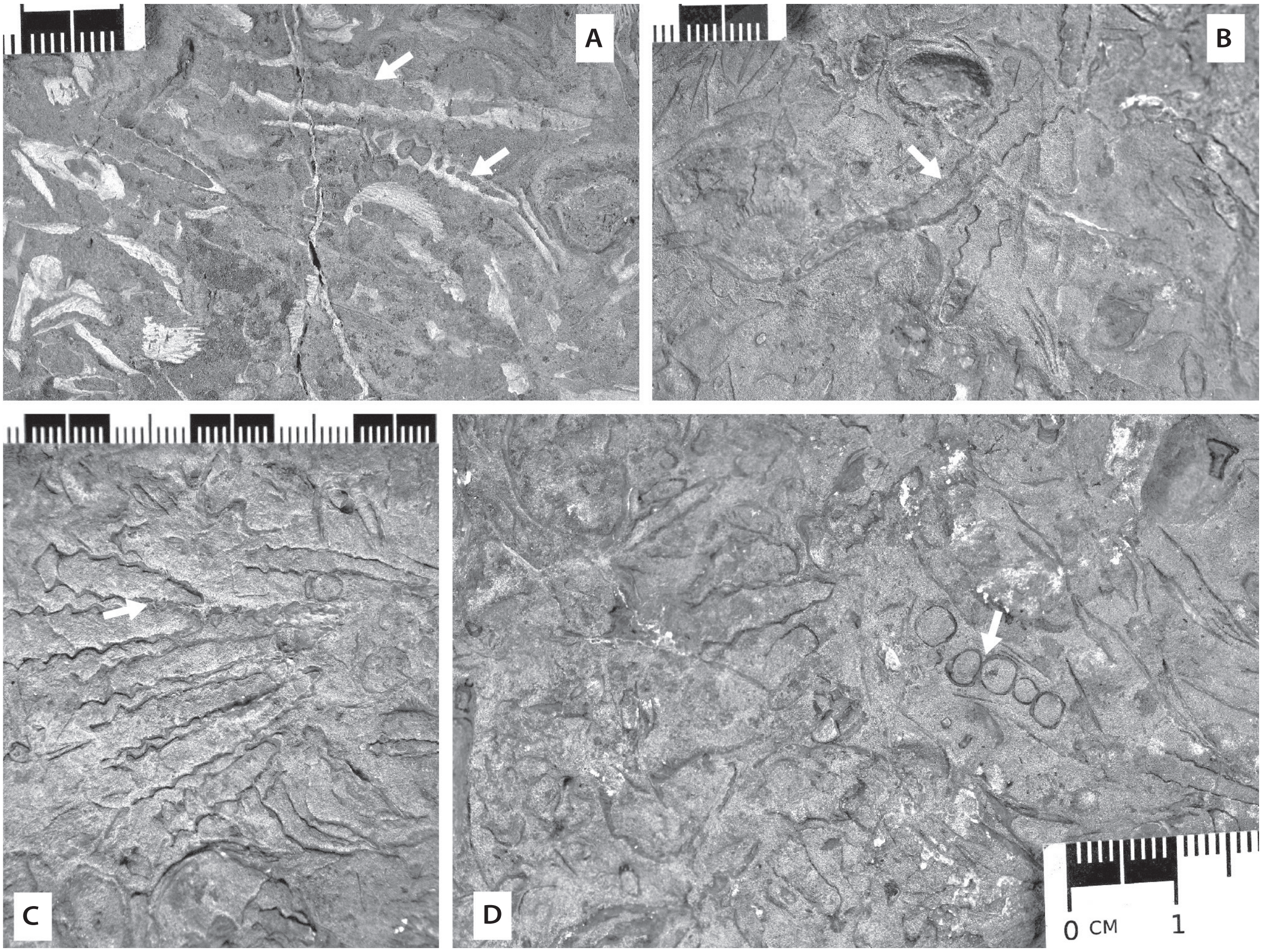

Figure 7. Details of cornulitids at the top surface of a shell bed of facies F6b sampled at 41 m (see outcrop in Fig. 5A). • A – the dominant species is *Cornulites gondwanensis* Gutiérrez-Marco & Vinn, 2018 (arrow). • B – another species with sinuous tube: *Cornulites* aff. *shallochensis* Cowper Reed, 1923 (arrow). • C – aggregated cornulitids recumbent in the bed surface, forming a bundle with tube apex oriented to the right. • D – aggregated specimens preserved in their original vertical position (arrow). This was interpreted after tomographic analysis (see text).

Shell beds in outcrop

The shell beds are discrete dm-thick layers forming either a unique stratigraphic marker (F6a, F6c) or amalgamated laterally within a facies unit that can be traced over kilometers (F6b).

F6a: This facies occurs in a single occurrence, in the form of a conglomerate preserved above an erosion surface scouring F3 shoreface deposits, and overlain by a flat-toped sandstone with faint horizontal bedding (Fig. 4; Fig. 5C, D). The elements of the conglomerate, a few cm in diameter, subangular to subrounded, have a sandstone lithology similar to that in F3. The matrix of the conglomerate is a packstone with a silty matrix. Bioclasts in the packstone contain mm- to cm-sized fragments of brachiopods, trilobites, crinoids, gastropods and cornulitids. The brachiopod bioclasts that are flaky are commonly packed into clusters with imbrications inclined in alternate apparent directions (Fig. 5E). Change in imbrication occur across faint stratification surfaces where the flaky bioclasts are mostly horizontal. This fabric is further documented in tomographic images (see below).

F6b: This facies occurs in 3 occurrences along the section (Fig. 4). It is composed of bioclastic layers (shell beds) conformably interstratified with fine sandstone in the infilling of troughs about 1 m deep and up to 20 m wide, forming a cut-and-fill architecture with up to 7 bedsets. These deposits are encased in F5 foreshore deposits along

reverse flows (arrows). • D – last occurrence of shell bed at 55 m (arrow). This one is a single thin pavement of entire shells (F6c). It seals a prominent sandstone bed with SCS (F4). • E – detail of the top surface of the shell bed illustrated in Fig. 6D. Note the clasts (arrow). • F – further detail on this surface, showing perfectly preserved cornulitids (Co) and brachiopods (Br).

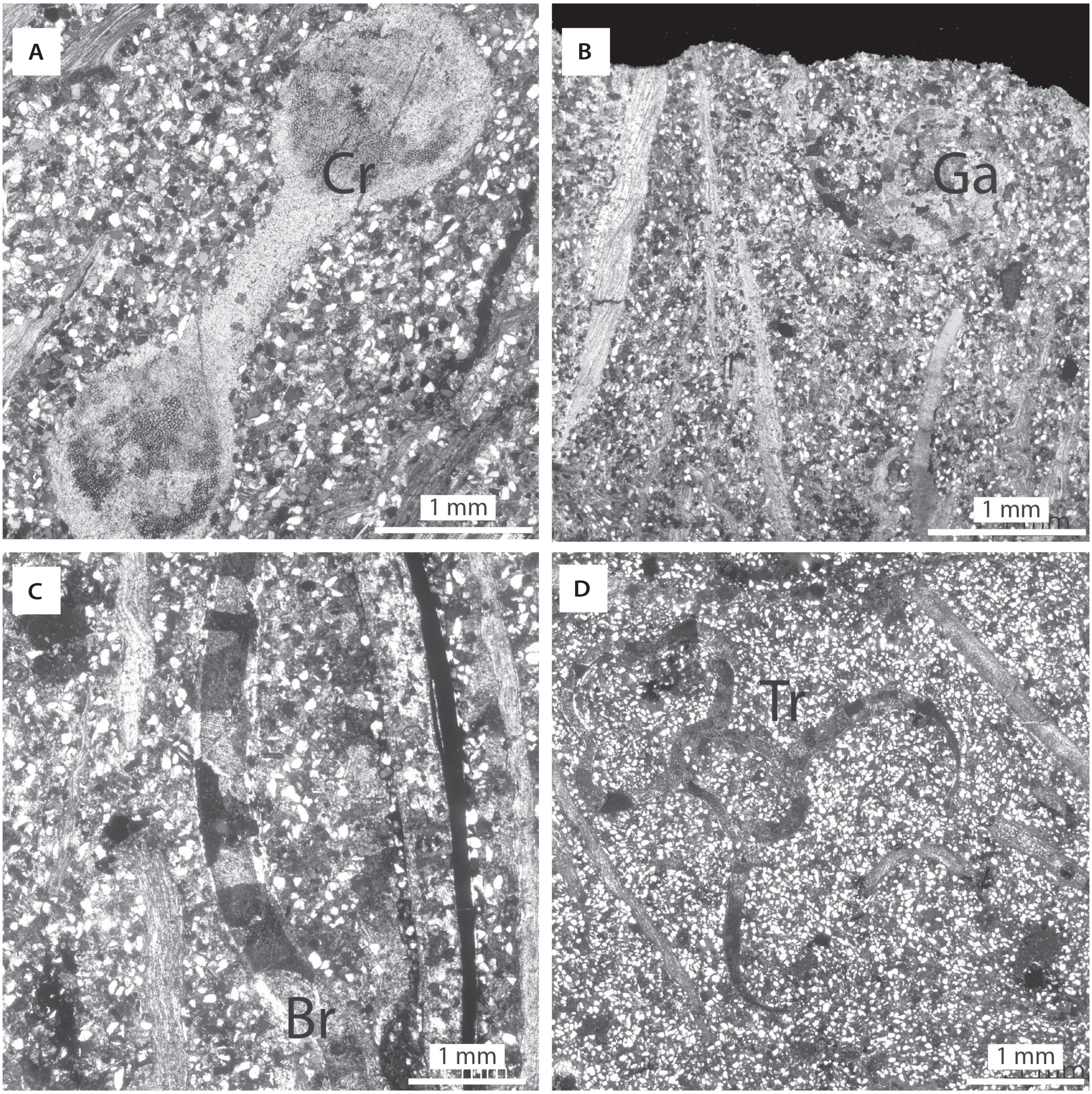

Figure 8. Thin sections from the shell bed of Fig. 6, showing the silty matrix with carbonate cement. Most bioclasts can be identified. • A – crinoids (Cr). • B – gastropods (Ga). • C – brachiopods (Br). • D – trilobite (Tr).

an erosional surface floored by gutter casts (Fig. 6A). The internal structure of the shell beds is similar to that in facies F6a (compare Fig. 6C and Fig. 5E). The sandstone has faint lamination locally underlined by veneers of entire shells (or their casts) and cornulitids. This lamination is either parallel to the lower bedset boundary or with low-angle tangential terminations (Fig. 6A). Bedsets locally truncate each other so that the shell beds can be overscoured. There is an overall upward thinning trend of the successive shell beds in the bedsets (Fig. 4).

F6c: This facies constitutes the last stratigraphic occurrence of a shell bed along the section, preserved above a prominent bed of F4 upper shoreface deposits where SCS passes upward to upper plane bedding (Fig. 6D). Facies F6c is composed of a 5-cm-thick pavement of cornulitids and brachiopods perfectly preserved within a muddy matrix (Fig. 6E, F). Bioclastic fragments are almost absent, unlike in facies F6a and F6b. The top of this bed forms a firm- or hardground with some mudclasts (Fig. 6E). In some places, the surface is sliced so that fossils

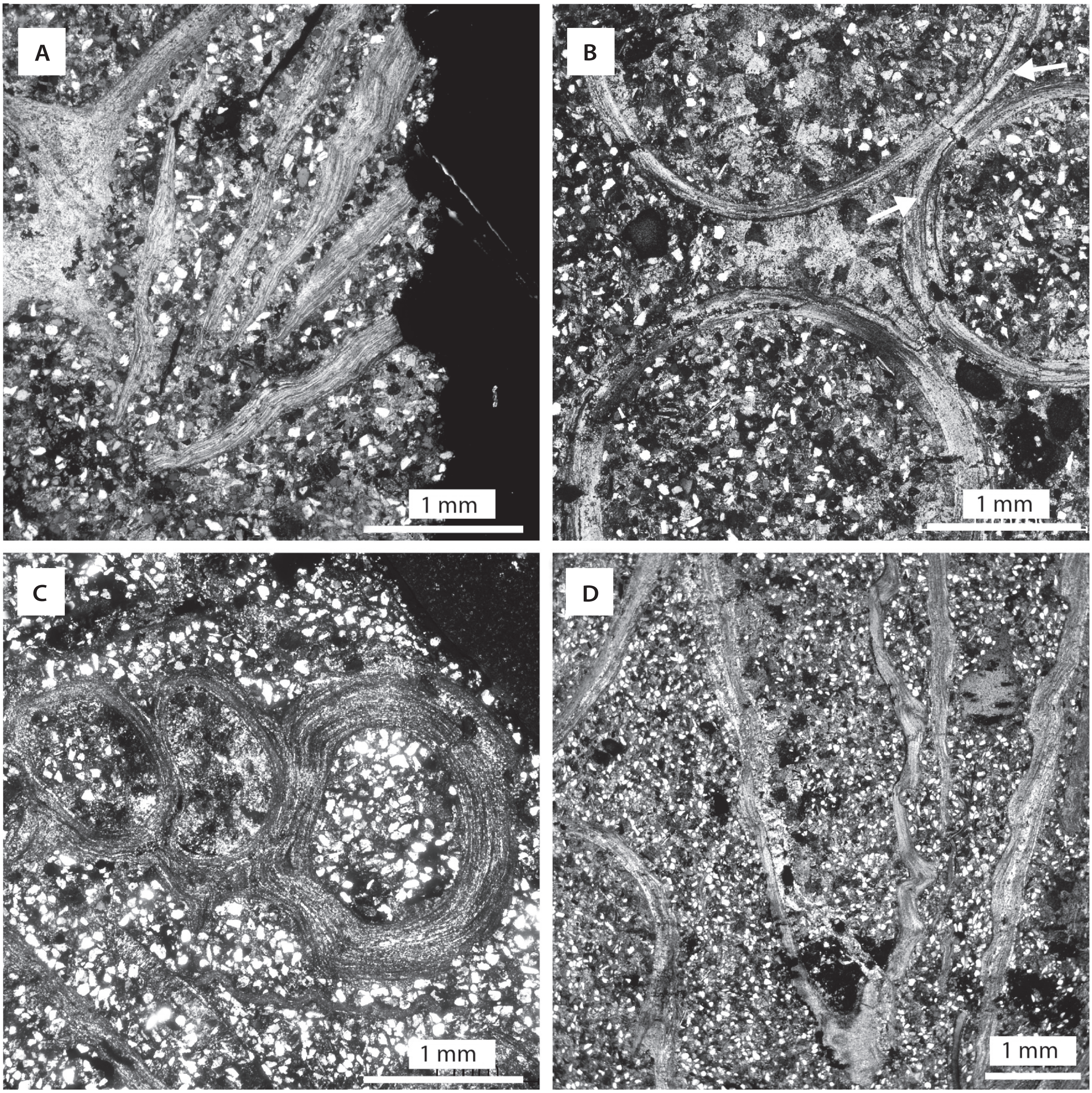

Figure 9. Cornulitids in thin sections, from the same sample as in Fig. 6. • A – longitudinal section of an aggregate of recumbent tubes (section parallel to bedding). • B – cross sections of aggregated (top) or only juxtaposed (bottom) tubes. In aggregates, the outer layer passes from one tube to the other (arrows). • C – longitudinal cross section away from the tube axis. The apparent cells are the annuli of the tube. • D – longitudinal section of specimens showing their annulated wall.

appear in cross sections (Fig. 6E), while in other places they were preserved in 3D beneath facies F1 (Fig. 6F).

Interpretation. – The interpretation of shell beds in terms of depositional environment is crucial to better understand the position of ecosystems in the depositional profile. The shell beds in facies F6a and F6b are interstratified in sandstones deposited in a high energy setting above a prominent erosion surface. The horizontal bedding in the sandstone comprising the F6a shell bed is interpreted as upper-plane bedding, indicating a foreshore setting, likely in the swash zone (Clifton *et al.* 1971). The cut-and-fill of troughs in facies F6b is interpreted as large-scale SCS, suggesting a shoreface setting. The occurrence of shell veneers in diasthems of HCS/SCS has been noted for a long time (Dott & Bourgeois 1982). The 20 m-wide scour depressions floored by gutter casts would result from storm-wave erosion. The generation of such very large-scale scour depressions by storms and then infilled by 3D bedforms corresponding to HCS has been described from sea-floor images and box cores of the lower shoreface (16–18 m water-depth) of Southern North Sea (Passchier & Kleinhans 2005). Thus, the shell beds in F6a and F6b can be considered as shoreface to foreshore storm beds (reworked thanatocenosis). Only the shells in F6c might be in place, thus in a more distal part of the depositional profile. This is the kind of type-b shell bed reported in Upper Ordovician deposits of Anti-Atlas by Botquelen *et al.* (2004, 2006). Their concentration along with clasts in a hard ground either suggests that energy was too low for the shells to be broken into bioclasts, or that condensation occurred due to winnowing of bioclasts. In both cases, this suggests that the biotope of F6a and F6b shell beds could lie in the offshore transition.

Shell bed microfacies

A full assessment of the taphonomy of those shell beds is beyond the scope of this article. While examining them, it appeared that cornulitids could be an interesting perspective as regarding to the ecology of the biota associated to the shell beds, as they had not been observed before in the Upper Ordovician of Algeria.

Cornulitid tubeworms belong to the class *Tentaculita* (Vinn & Zatoń 2012). These suspension-feeding lophophorates are the only fossils that are preserved as entire specimens and not broken into bioclasts, despite their fragile structure. Brachiopods can be found as entire valves, or, when broken, large fragments. This suggests that the cornulitids lived at or in the vicinity of the site of their deposition. Their mass occurrence can provide information on their autoecology. A sample taken from the F6b shell bed at 41 m was studied in detail.

Cornulitids observed at the bed surface

The top bedding surface of the sample, corresponding to the abandonment surface of the shell bed below the overlying sandstone facies (Fig. 6A) shows a high density packing and a very low diversity of cornulitids. Two species are observed: (i) *Cornulites gondwanensis* (Gutiérrez-Marco & Vinn 2018) (Fig. 7A). They are tubes up to 40 mm long with up to 4.0 mm wide apertures, straight to almost straight. Tubes covered externally with prominent well-developed and regularly shaped annulations. Tubes do not bear attachment scars and have no widened tube bases, suggesting they were solitary and not attached to the ground. (ii) *Cornulites* aff. *shallochensis* Cowper Reed, 1923 (Fig. 7B). These specimens have a slightly sinuous, relatively large tube (*i.e.*, 35 mm long) with irregular annuli of variable development. Besides the fact that those two species appear to live as free forms, groups of 4–6 specimens form bundles where the tubes are in the same plane, with their apertures in the same direction (Fig. 7C). Such tube aggregates were likely formed when the animals had an upright living position in the sediment, with the aperture at the sediment-water interface allowing most efficient suspension feeding. Aggregates of tubes preserved in a vertical position are inferred by series of contiguous cells (Fig. 7D), but whether apertures are oriented upwards cannot be determined at this stage.

Petrography in thin sections

Observation of the thin sections of the above sample of F6b shell bed reveals that the shell bed matrix contains more than 60% angular to sub-angular quartz grains, with an average size of 50 μm (Fig. 8). Micas, mainly muscovite, are also present. Feldspar, when present, show significant alteration. The cement is carbonated, probably resulting from the dissolution of the shells. Examination of the thin sections also confirms the presence among bioclasts of echinoderm plates (Fig. 8A), gastropods (Fig. 8B), brachiopods (Fig. 8C) and trilobites (Fig. 8D).

The thin sections show several longitudinal and transverse sections of the cornulitids, revealing the tube aggregates already observed on the bed surface (Fig. 9A, B). Longitudinal sections show that the wall structure is formed of several layers, with centripetal concentric growth (the initial layer constituting the outer layer) (Fig. 9C, D). Some aggregated tubes have an outer layer in common (Fig. 9B). This structure explains how tubes in aggregates can be welded and possibly then transported as clusters.

Shell-bed fabric in tomography

Examination of the sample by 3D tomography reveals multiple positions of the cornulitid tubes buried in the sediment, with their aperture oriented upwards or downwards, or the tubes recumbent in the bed (Fig. 10A). The upward aperture probably corresponds to the dwelling position of filter-feeding individuals. As lophophorates, cornulitids were incapable of burrowing with their aperture downwards. Therefore, the specimens with downward oriented aperture or lying on the bed resulted from post-mortem transportation and sedimentation. The recumbent specimens have random orientations in the bed (Fig. 10B), so that their section can be circular, as observed in the field (Fig. 5E). Tomographic images clearly show that these correspond to cornulitids (Fig. 10C). Where the recumbent cornulitids are elongated along the paleoflow, their apices generally indicate the lee, as it can be deduced coincidentally by imbrication of the flaky brachiopod bioclasts (Fig. 10D). The vertical tomographic sections

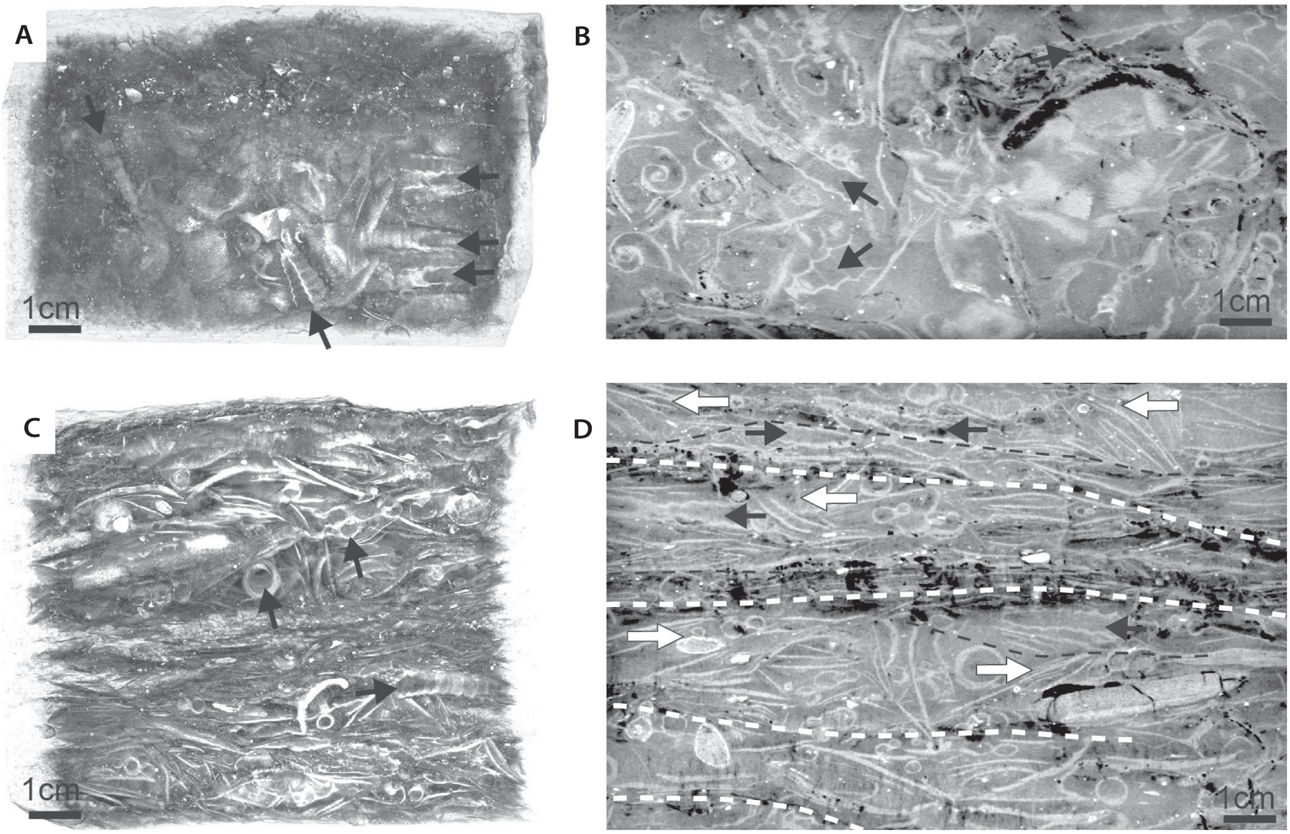

Figure 10. Tomographic images of a 10 × 7 × 5 cm block extracted from the sample shown in Fig. 6. • A – 3D view of a vertical slice located at the core of the sample. Most of cornulitids are found recumbent in the bed but some with their apex oriented upwards or downwards (arrows). • B – horizontal section showing that the cornulitids recumbent in the bed may be oriented in various directions. • C – 3D view showing that the circular sections correspond to cornulitids (arrows: see their annulated inner surface). • D – vertical section showing the typical rhythmic layering of shells, as observed on the field. The dotted lines highlight veneers where the flaky bioclasts are parallel to the bed. They delineate undulated bedforms. White arrows show paleoflows as deduced from bioclast imbrications. Black arrows point to the wider, open end of cornulitid tubes. White dashed lines show flow reversal surfaces.

provide further details on the stratification observed in the field (compare Figs 4E, 5C and 9D). Stratification is formed by alternation of up to 5 cm wavy layers separated by veneers of flat-lying bioclasts (Fig. 10D). Paleoflow reversal occurred from one layer to the other, and possibly laterally where wavy layers crosscut each other.

Discussion

Shell beds in transgressive ravinements

The association between shell beds and high-frequency variations in sea level has been well documented in the Ordovician (Botquelen *et al*. 2004, 2006; Álvaro *et al.* 2007 a, b; Loi *et al*. 2010; Colmenar & Álvaro 2015; Vaucher *et al.* 2016). The logged succession is interpreted as a stack of 11 high-frequency sequences (Zecchin & Catuneanu 2013). These sequences are 5 m thick on average across the 55 m of the lower part of the logged section. Considering that the Hassi Chaamba Fm., about 600 m thick (Fig. 2), comprises the Darriwilian and Sandbian (14 Myrs according to Gradstein *et al*. 2012), this suggests an average sedimentation rate of about 42 m/Myr. Thus, each of the 11 sequences would have a duration of 0.118 Myr, which is close to the period of eccentricity cycles of the Earth's orbit. This suggests that these sequences are controlled by glacioeustatic sea-level changes.

The sequences are mostly composed of conformable regressive system tracts ranging from F1–F2 offshore deposits to F3–F4 shoreface deposits, and ultimately to F5 foreshore deposits (Fig. 4). This fits to the classic wave-dominated ramp model of progradational siliciclastic shelves (Walker 1984, 1992; Brenchley *et al*. 1986; Boyd *et al*. 1992). The F6 shell beds are bounded at the base by a sharp, erosional surface (*e.g.*, Figs 5D, 6A). The through of SCS in F6b shell beds are about 5 m in wavelength, twice as large as the largest HCS/SCS preserved in the F3–F4 shoreface deposits. Although HCS may result from the combination of oscillatory and steady flows (Sherman & Greenwood 1989), the wavelength of the hummocks and swales must be scaled to the orbital diameter of the waves, as for vortex ripples, and therefore to water depth. This implies a sharp increase in water depth across the erosional boundary at the base of the shell beds. This erosion surface is thus interpreted as a transgressive ravinement surface, and the overlying shell beds and embedding deposit as a thin, transgressive system tract. The transgressive ravinement would possibly rework lithified sediments, as evidenced by the sandstone clasts in the F6a shell bed (Fig. 5C), or the gutter casts at the bottom of F6b (Fig. 6A), suggesting it could be amalgamated with a subaerial unconformity.

The sequence stacking pattern shows two overall regressive sequence sets (Fig. 4). The thickness and proportion of proximal facies increases in the sequences upward the regressive sequence sets. The lower one ends at 20 m, with amalgamated beds of F4 upper shoreface deposits. The upper one, ending at 48 m, is composed of thicker sequences, the regressive system tract of which grades up to F5 foreshore deposits. Therefore, this sequence set overall might record a larger regression, with possible relative sea-level falls recorded as regressive surfaces of marine erosion at the erosional base of foreshore deposits. The last sequence, from 48 m to 55 m, comprises an in-situ thanatocenosis preserved in F6c (Fig. 6F) and sealed as hardground beneath F1 offshore shales. This suggests that the shelly fauna was primarily living in the offshore transition. Its occurrence in the sequences below as reworked F6a–b shell beds suggest that, at onset of transgression and during extreme storms, the biotope could be hit by the largest waves. In the last sequence, sea level did not fall low enough to allow this. The logged section above this last sequence (Fig. 4; from 55 m to 95 m) further shows a complete change in facies organization that is thought to reflect an overall transgression (Metatla 2023). As a consequence, the shell beds are preserved in a turnaround from a regressive to transgressive sequence set.

A facies model of the Hassi Chaamba shell beds is proposed (Fig. 11). This model shows the geometrical relationships of facies observed in the shell-bed bearing sequences, integrated in a dip section of the coastal profile. It also shows two erosion surfaces. The regressive surface of marine erosion is mostly inferred from the absence of F4 upper-shoreface deposits below the F6b shell beds. By contrast, the transgressive ravinement surface is the most prominent erosion surface, that is supposed to truncate the former in the proximal part of the profile. The relative location of facies F6a and F6b is not constrained, as F6a could be a lateral equivalent or inter-trough expression of facies F6b, instead of a proximal counterpart. By contrast, F6c is assumed to correspond

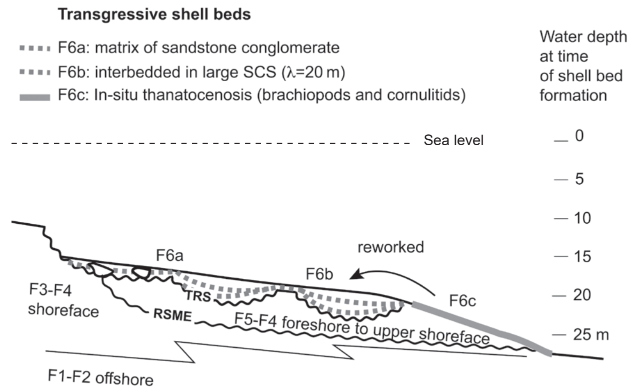

Figure 11. Facies model of the Hassi Chaamba shell beds proposed in this study. All facies are primarily controlled by storms. The regressive facies tract F1–F4 is present in all sequences, while the foreshore F5 is observed only below and within the F6 shell beds. The shells are reworked into F6a–b transgressive storm beds in the shoreface and preserved in place as a F6c hardground deeper in the profile. The F4–F5 beds below the shell beds point to a downward shift of facies, that can be the result of a forced regression before transgression. The shelly fauna biotope expands from the offshore to possibly the shoreface where some shells might be reworked in place. Tidal dynamics possibly controls the inner bedding of storm beds, as supposed from that of the shell beds.

to the deeper part of the profile, below the storm wave-base. The model implies an increase of wave size during transgressions, in response to increase in water depth. Transgressive ravinement would also favor the change from a convex- to concave-up shoreface profile, and thus allow larger waves to impinge the shoreface. The biotope of the shelly fauna would mainly lie in the offshore transition, but the supply of shells to the shoreface would be facilitated by the Stokes drift of the storm waves (Allen 1997). Following the typology of Kondo *et al.* (1998), the shell beds in F6a–b are "onlap" shell beds, while the one in F6c is a "backlap" shell bed. The reason why neither sparse shells nor shell beds are found in the shoreface deposits of the regressive systems tracts remains open, but may owe to the relationships between hydro-sedimentary dynamics and ecology in the coastal zone.

Autoecology and biota behavior

From an autoecological perspective, the oligospecificity of the preserved biota suggests a stressed environment with trophic conditions restricted in time. The biota could radiate across the profile during short periods and the shelly material be quickly reworked and buried in storm deposits. This applies to entire brachiopods that are preserved in the shell beds, together with gastropods and cornulitids. Besides, since the brachiopods are the source of large amounts of flaky bioclasts forming the bulk of the shell beds, they could be reworked through longer periods and present over larger areas.

The occurrence of cornulitids aggregates implies that reworking was not able to dislocate them, although the welding might be very fragile. This suggests that especially for those biota reworking was minor, meaning that they were living in the shell bed between storms. Some cornulitids could grow partially buried with their proximal end in the sediment. Such life mode presumably represents an adaptation to high hydrodynamic conditions and little hard substrate. The formation of aggregates thus could be a way for them to better anchor to the bed (Vinn 2010). The primary position would be with an aperture of the worm tube slightly above the water-sediment interface, allowing the organism to filter food particles from the water column. Aggregates buried in the sediment with apertures oriented upward are observed in F6b shell beds, suggesting they are preserved in living position. The cornulitids have a recumbent position in F6c, where the position of their aggregates suggests that the organisms were lying dead on the firm seafloor. The latter preservation is consistent with the thanatocenosis interpretation of this shell bed. In case of post mortem displacement, the aggregations would have been reworked and deposited with the heavier apertural part down, and this should have happened in a soft sediment. Tomography data of F6b shell beds show cornulitids tubes oriented like this, but preserved together with tightly packed and imbricated brachiopod shells, which is not consistent with a soft bed. The shell bed texture suggests that the shells could have been partially lifted by turbulence and/or packed obliquely again objects protruding from the bed. The latter possibility is illustrated by some tomographic sections (see Fig. 10D, lowermost arrow). The occurrence of entire cornulitid aggregates in life position could thus be a coincidence, but also a hint that they were capable of restoring their life position with apertures oriented upwards, possibly after the peak energy event, and provided they were not buried in the meantime. Such ability to correct orientation occurs in modern polychaete tubeworm *Ditrupa* (Hove & Smith 1990) which would be the best modern analogue to cornulitids anchored with their tubes in soft sediment.

The role of tides

The very good preservation of fragile cornulitid tubes in F6b shell beds is striking, considering that they lie in storm beds forming very-large SCS. The internal geometry of the SCS in facies F6b shows oblique low-angle crossbedding, a feature typical of anisotropic HCS/SCS which indicates combined flows (*e.g.*, Arnott & Southard 1990). The unidirectional flow component could be either tidal, or rip currents induced by storm downwelling (Dumas & Arnott 2006). We hypothesize that tidal dynamics is possibly recorded in the facies geometry and succession encompassing the shell beds.

The large-scale SCS infilling the troughs in F6b shell beds are floored by fining-up shell beds, conformably overlain by sand, suggesting a decrease in shell supply and energy recorded during deposition of each of the sets forming the cut-and-fill architecture of this facies. Up to 7 cycles of cut-and-fill are observed in F6b shell bed occurrences. These cycles could be punctuating the waning stage of a single big storm, as in the original model of Dott & Bourgeois (1982), or a succession of storms. In the first hypothesis, the full cut-and-fill package (up to 1m) would be deposited within a few days and the shell beds inside each bedset could reflect daily tidal cycles. In the second hypothesis, the shell beds would represent the climax of each storm, with a possibly long time (decades, centuries?) between them. There are two points in favor of the single storm hypothesis for each bedset. First, the troughs infilled by each bedset are of comparable depth as the thickness of the full cut-and-fill unit, which in turn compares with the amplitude of the large scour hollows at the bottom. Those scours do not argue in favor of a long-lasting levelling of this surface under the erosive action of waves. Second, the layering within the shell beds shows a rhythmic change in hydrodynamics, following an alternation of stages of flattening and lifting of bioclasts. The layers with lifted bioclasts would reflect a stronger advection into eddies while they move along the bed. Their imbrication shows reverse flows on vertical sections, but with random directions on horizontal slices (Fig. 10B). This may be due to the oscillatory component of waves. However, the layers with flat bioclasts are also with more matrix, suggesting a decrease in energy not consistent with maintenance of the orbital motion. The stages of flattening could reflect lesser stirring due to oscillation. These rhythmic changes in energy during infilling of a single swale of the SCS suggest that they were fast, must faster than the lateral shifting of the orbital cell that created the structure. We hypothesize that this could be the time-scale of daily tides.

Significant changes in water depth could be responsible for those changes. Because waves in shallow water are scaled to water depth, orbital diameter of waves formed at high tide must be larger than that of waves formed at low tide. Increased water depth, however, reduces the impact of waves at the sea bed. For bedforms of tempestites in the shoreface- to offshore transition, Vaucher *et al*. (2017) hypothesized that wave effect should be larger at low tide. In the surf to swash zone, however, the contrary is more likely. As predicted by the tidally modulated shoreface model Dashtgaard *et al*. (2009), the larger bedforms preserved on macrotidal wave-dominated foreshores must be formed during high tide. This is also documented in modern open-coast tidal flats (Yang *et al*. 2006). Although this example refers to pure tidal flat, tidal facies formed at low tide in such environments have little chance to be preserved, and most of the lower intertidal record is composed of HCS (Li *et al*. 2000, Fan *et al.* 2004, Yang *et al*. 2005).

From a sequence stratigraphic perspective, inferring the interplay of tides in F6b shell beds is consistent with their location on transgressive surfaces. During transgressions, the increase in width of the shelf commonly favors tidal resonance, which would increase the tidal range at the coast (Reynaud & Dalrymple 2012). There are unfortunately no data about the paleogeography of the basin that would allow to calculate its resonance period and to compare it with the semi-diurnal tidal period. The sandstones that crop out above the shell beds in the logged section (58–93 m, Fig. 4) do not show evidence of wave dynamics, but there are some hints that they could be tidal deposits (Metatla 2023): (i) they are coarser, such as expected by transgressive winnowing of clastics supplied at the coast; (ii) they contain marine fossils, including the species of the shell beds, and are pervasively bioturbated with marine trace fossils; (iii) they are entirely cross-bedded at various scales, locally pointing to large-scale bedforms evolving in subcritical flows. Some of these sandstones at least share common features with tidal sand sheets as reported by Stride (1982), or tidal bars and dunes as reported by Dalrymple & Rhodes (1995).

In the rock record, numerous studies suggest a tidal modulation in the HCS, and this always implies a large tidal range (Plink-Björklund 2008, Basilici *et al*. 2012, Vakarelov *et al*. 2012, Rossi & Steel 2016, Vaucher *et al*. 2017). Closer to the study area, the presence of hybrid wave/tide facies has already been noted in the Bou M'Haoud formation of the Saoura range (Ghienne *et al.* 2007) and in the Ordovician of Morocco (Marante 2008, Loi *et al.* 2010, Meddour 2016, Vaucher *et al.* 2017). The novelty in the Daoura shell beds is the perspective that this hypothesis brings to autoecology of the shallow-marine biota.

Conclusion

A 55-m thick section of the middle part of the Hassi Chaamba Fm. exposed in Djebel Moussine was studied in detail. It consists of siliciclastic facies ranging from the offshore transition to the foreshore of a wave-dominated ramp. The facies tract forms high-frequency sequences (~100 ka), each up to 10 m thick, organized in regressive-transgressive sequence sets. The sequences at the turn-around from a regressive to transgressive sequence set comprise shell beds. The shell beds are present in transgressive lags, as reworked (foreshore to shoreface) or in-situ thanatocenosis (offshore transition). All shell beds comprise the same biota, dominated by brachiopods (forming most bioclasts) and cornulitids (unbroken). The shell beds in shoreface deposits are interstratified in very-large SCS which infill scour depressions, 20 m in wavelength. These deposits reflect an increase of the size of storm waves at the coast, a consequence of increased accommodation during transgression. These transgressive shell beds would reflect a change from wave dominance to increasing tidal influence. The layering of shell beds in the SCS reflects variation of energy that may be driven by daily changes in water depth controlled by the tide. Tomographic images of the shell beds show an internal layering that can also reflect cyclic changes of the intensity of stirring at the bed within the time of a single storm. The wave-current combination is also deduced from (i) interstratification of upper-plane beds above or below the shell beds, and (ii) the dominance of anisotropic HCS (lateral accretion). Tomographic images demonstrate a perfect preservation of cornulitids in various orientations inside the shell beds. This suggests that they were moved together with the bioclasts. However, some tubes are aggregated, which is an adaptation to loose grounds. The maintenance of some aggregates with upright aperture of the tubes is unlikely unless they could restore a living position between two agitation periods (possibly two tides). These results open new perspectives on the auto-ecology of shell-bed biota and the deconvolution of tidal signatures in storm beds.

Acknowledgments

This work was funded by the French Ministry of Foreign Affairs (Campus France – ProfasB+; scholarship of Imène Metatla) and CNRS-INSU (TelluS Syster program; field work and analyses). The authors would like to thank two anonymous reviewers for their constructive reviews.

References

Ait Kaci, A. 1990. *Evolution lithostratigraphique et sédimentologique des Monts d'Ougarta pendant le Cambrien (Sahara algérien nord occidental)*. 193 pp. Ph.D. thesis, Université des sciences et de la technologie Houari Boumediene, Algiers, Algeria.

Allen, P.A. 1997. *Earth surface processes*. 404 pp. Blackwell Science. DOI 10.1002/9781444313574

Altumi, M.M., Elicki, O., Linnemann, U., Hofmann, M., Sagawe, A. & Gärtner, A. 2013. U–Pb LA-ICP-MS detrital zircon ages from the Cambrian of Al Qarqaf Arch, central-western Libya: Provenance of the West Gondwanan sand sea at the dawn of the early Palaeozoic. *Journal of African Earth Sciences 79*, 74–97. DOI 10.1016/j.jafrearsci.2012.11.007

Álvaro, J.J., Aretz, M., Boulvain, F., Munnecke, A., Vachard, D.

& Vennin, E. 2007a. Fabric transitions from shell accumulation to reefs: an introduction with Palaeozoic examples. *Geological Society- Special Publication 275*, 1–16. DOI 10.1144/GSL.SP.2007.275.01.01

Álvaro, J.J., Vennin, E., Villas, E., Destombes, J. & Vizcaino, D. 2007b. Pre-Hirnantian (slatest Ordovician) benthic community assemblages: Controls and replacements in a siliciclastic-dominated platform of the eastern Anti-Atlas, Morocco. *Palaeogeography Palaeoclimatology Palaeoecology 245*, 20–36. DOI 10.1016/j.palaeo.2005.09.035

Álvaro, J.J., Benharref, M., Destombes, J., Gutiérrez-Marco, J.C., Hunter, A.W., Lefebvre, B., Van Roy, P. & Zamora, S. 2022. Ordovician stratigraphy and benthic community replacements in the eastern Anti-Atlas, Morocco, 37–67. *In* Hunter, A.W., Álvaro, J.J., Lefebvre, B., Van Roy, P. & Zamora, S. (eds) *The Great Ordovician Biodiversification Event: Insights from the Tafilalt Biota, Morocco*, *Geological Society London, Special Publication 485*. DOI 10.1144/SP485.20

Arnott, R.W. & Southard, J.B.1990. Exploratory flow-duct experiments on combined-flow bed configurations, and some implications for interpreting storm-event stratification. *Journal of Sedimentary Research 60*, 211–219. DOI 10.1306/212F9156-2B24-11D7-8648000102C1865D

Askri, H., Belmecheri, A., Benrabah, B., Boudjema, A., Boumendjel, K., Daoudi, M., Drid, M, Ghaalem, T., Docca, A.M., Ghandriche, H., Ghomari, A., Guellati, N., Khennous, M., Lounici, R., Naili, H., Thakerist, D. & Terkmani, M. 1995. Geology of Algeria, 1–93. *In* Delsol, D. (ed.) *Well Evaluation Conference Algeria*. Houston, Schlumberger.

Avigad, D., Sandler, A., Kolodner, K., Stern, R.J., Mcwilliams, M., Miller, N. & Beyth, M. 2005. Mass-production of Cambro-Ordovician quartz-rich sandstone as a consequence of chemical weathering of Pan-African terranes: Environmental implications. *Earth and Planetary Science Letters 240*, 818–826. DOI 10.1016/j.epsl.2005.09.021

Baidder, L., Michard, A., Soulaimani, A., Fekkak, A., Eddebbi, A., Rjimati, E.-C. & Raddi, Y. 2016. Fold interference pattern in thick-skinned tectonics; a case study from the external Variscan belt of Eastern Anti-Atlas, Morocco. *Journal of African Earth Sciences 119*, 204–225. DOI 10.1016/j.jafrearsci.2016.04.003

Basilici, G., De Luca, P.H.V. & Oliveira, E.P. 2012. A depositional model for a wave-dominated open-coast tidal flat, based on analyses of the Cambrian-Ordovician Lagarto and Palmares formations, north-eastern Brazil. *Sedimentology 59*, 1613–1639. DOI 10.1111/j.1365-3091.2011.01318.x

Bassis, A., Hinderer, M. & Meinhold, G. 2016. Petrography and geochemistry of Palaeozoic quartz-rich sandstones from Saudi Arabia: implications for provenance and chemostratigraphy. *Arabian Journal of Geosciences 9*, 400. DOI 10.1007/s12517-016-2412-z

BEICIP 1972. *Etude Géologique et Levers Cartographiques au 1/200 000 de la Daoura (Sahara occidental)*. Report 30463.

Botquelen, A., Loi, A., Gourvennec, R., Leone, F. & Dabard, M.-P. 2004. Formation et signification paléo-environnementale des concentrations coquillères: exemples de l’Ordovicien de Sardaigne et du Dévonien du Massif armoricain. *Comptes Rendus Palevol 3(5)*, 353–360. DOI 10.1016/j.crpv.2004.06.003

Botquelen, A., Gourvennec, R., Loi, A., Pillola, G.L. & Leone, F. 2006. Replacements of benthic associations in a sequence stratigraphic framework, examples from Upper Ordovician of Sardinia and Lower Devonian of the Massif Armoricain. *Palaeogeography Palaeoclimatology, Palaeoecology 239*, 286–310. DOI 10.1016/j.palaeo.2006.01.016

Boumendjel, K., Brice, D., Copper, P., Gourvennec, R., Jahnke, H., Lardeux, H., Menn, J., Melou, M., Morzadec, P., Paris, F., Plusquellec, Y. & Racheboeuf, P. 1997. Les faunes du Dévonien de l’Ougarta (Sahara occidental, Algérie). *Annales de la Société Géologique du Nord 5*, 89–116.

Boyd, R., Dalrymple, R. & Zaitlin, B.A. 1992. Classification of clastic coastal depositional environments. *Sedimentary Geology 80*, 139–150. DOI 10.1016/0037-0738(92)90037-R

Brahimi, S., Liégeois, J.-P., Ghienne, J.-F., Munschy, M. & Bourmatte, A. 2018. The Tuareg shield terranes revisited and extended towards the northern Gondwana margin: Magnetic and gravimetric constraints. *Earth-Science Reviews 185*, 572–599. DOI 10.1016/j.earscirev.2018.07.002

Brenchley, P.J., Romano, M. & Gutierrez-Marco, J.C. 1986. Proximal and distal hummocky cross-stratified facies on a wide Ordovician shelf in Iberia, 241–255. *In* Knight, R.J. & Mclean, J.R. (eds) *Shelf Sands and Sandstones*. *Canadian Society of Petroleum Geologists Memoir 11*.

Busson, G. 1972. *Principes, méthodes et résultats d’une étude stratigraphique du Mésozoïque saharien*, 441 pp. Mémoires du Muséum national d’Histoire naturelle, Série C. Paris.

Cheel, R.J. & Leckie, D.A. 1993. Hummocky Cross-Stratification, 103–122. *In* Wright, V.P. (ed.) *Sedimentology Review/1*. John Wiley & Sons. DOI 10.1002/9781444304534.ch7

Chikhaoui, M. & Donzeau, M. 1972. Le passage Précambrien-Cambrien dans les monts d’Ougarta: Le conglomérat du Djbel Ben Tadjine (Saoura, Sahara algérien nord-occidental). *Bulletin de la Société d’Histoire Naturelle de l’Afrique du Nord 63(1–2)*, 51–62.

Clifton, H.E. 1976. Wave-Formed Sedimentary Structures–A Conceptual Model. *In* Davis, R.A., Jr. & Ethington, R.L. (eds) *Beach and Nearshore Sedimentation, SEPM Special Publication 24*. DOI 10.2110/pec.76.24.0126

Clifton, H.E., Hunter, R.E. & Phillips, R.L. 1971. Depositional structures and processes in the non-barred high-energy nearshore. *Journal of Sedimentary Research 41*, 651–670. DOI 10.1306/74D72473-2B21-11D7-8648000102C1865D

Colmenar, J. & Álvaro, J.J. 2015. Integrated brachiopod-based bioevents and sequence-stratigraphic framework for a late Ordovician subpolar platform, eastern Anti-Atlas, Morocco. *Geological Magazine 152*, 603–620. DOI 10.1017/S0016756814000533

Colmenar, J., Villas, E. & Rasmussen, M.Ø. 2022. A synopsis of Late Ordovician brachiopod diversity in the Anti-Atlas, Morocco. *Geological Society London, Special Publication 485*, 153–163. DOI 10.1144/SP485.3

Coward, M.P. & Ries, A.C. 2003. Tectonic development of

North African basins. *Geological Society London, Special Publication 207*, 61–83. DOI 10.1144/GSL.SP.2003.207.4

Cowper Reed, F.R. 1923. New Fossils from Girvan. *Geological Magazine 60*, 268–276. DOI 10.1017/S0016756800085770

Craig, J., Thurow, J., Thusu, B., Whitham, A. & Abutarruma, Y. 2009. Global Neoproterozoic petroleum systems: the emerging potential in North Africa. *Geological Society London, Special Publication 326*, 1–25. DOI 10.1144/SP326.1

Dalrymple, R.W. & Rhodes, R.N. 1995. Chapter 13 Estuarine Dunes and Bars, 359–422. *In* Perillo, G.M.E. (ed.) *Developments in Sedimentology 53.* Elsevier. DOI 10.1016/S0070-4571(05)80033-0

Dashtgard, S.E., Gingras, M.K. & Maceachern, J.A. 2009. Tidally modulated shoreface. *Journal of Sedimentary Research 79*, 793–807. DOI 10.2110/jsr.2009.084

Dashtgard, S.E., Maceachern, J.A., Frey, S.E. & Gingras, M.K. 2012. Tidal effects on the shoreface: Towards a conceptual framework. *Sedimentary Geology 279*, 42–61. DOI 10.1016/j.sedgeo.2010.09.006

Davies, N.S. & Gibling, M.R. 2010. Cambrian to Devonian evolution of alluvial systems: The sedimentological impact of the earliest land plants. *Earth-Science Reviews 98*, 171–200. DOI 10.1016/j.earscirev.2009.11.002

Destombes, J. 1983. *Notice explicative de la carte géologique du Maroc au 1/200.000: Zagora-Coude du Dra.* 243 pp. Notes et Mémoires du Service Géologique. Rabat.

Destombes, J. 1985. Lower Palaeozoic rocks of Morocco, 91–336. *In* Holland, C.H. (ed.) *Lower Palaeozoic of north-western and west-central Africa*. Wiley.

Donzeau, M., Fabre, J. & Moussine-Pouchkine, A. 1981. Comportement de la dalle saharienne et orogenèse varisque. Essai d'interprétation. *Bulletin de la Société d'Histoire Naturelle d'Afrique du Nord 69*, 137–172.

Dott, R.H. & Bourgeois, J. 1982. Hummocky stratification: Significance of its variable bedding sequences. *Bulletin of the Geological Society of America 93*, 663. DOI 10.1130/0016-7606(1982)93<663:HSSOIV>2.0.CO;2

Dumas, S. & Arnott, R.W.C. 2006. Origin of hummocky and swaley cross-stratification – The controlling influence of unidirectional current strength and aggradation rate. *Geology 34*, 1073–1076. DOI 10.1130/G22930A.1

Elicki, O., Meischner, T., Gürsu, S., Ghienne, J.-F., Masri, A., Moumani, K.A. & Demircan, H. 2023. The Ordovician System in the Levant region (Middle East) and southern Turkey: review of depositional facies, fauna and stratigraphy. *Geological Society London, Special Publication 533*, 253–277. DOI 10.1144/SP533-2022-53

Ennih, N. & Liégeois, J.-P. 2001. The Moroccan Anti-Atlas: the West African craton passive margin with limited Pan-African activity. Implications for the northern limit of the craton. *Precambrian Research 112*, 289–302. DOI 10.1016/S0301-9268(01)00195-4

Eschard, R., Braik, F., Bekkouche, D., Rahuma, M.B., Desaubliaux, G., Deschamps, R. & Proust, J.-N. 2010. Palaeohighs: their influence on the North African Palaeozoic petroleum systems. *Geological Society London, Petroleum Geology Conference Series 7*, 707–724. DOI 10.1144/0070707

Fabre, J. 1988. Les séries paléozoïques d'Afrique: une approche. *Journal of African Earth Science 7*, 1–40. DOI 10.1016/0899-5362(88)90051-6

Fabre, J. & Kazi-Tani, N. 2005. Ordovicien, Silurien, Devonien, Permo-Carbonifère. Géologie du Sahara occidental et central. *Tervuren African Geoscience Collection 108*, 227–240.

Fan, D., Li, C. & Wang, P. 2004. Influences of storm erosion and deposition on rhythmites of the upper Wenchang Formation (Upper Ordovician) around Tonglu, Zhejiang Province, China. *Journal of Sedimentary Research 74*, 527–536. DOI 10.1306/010304740527

Galeazzi, S., Point, O., Haddadi, N., Mather, J. & Druesne, D. 2010. Regional geology and petroleum systems of the Illizi–Berkine area of the Algerian Saharan Platform: An overview. *Marine and Petroleum Geology 27*, 143–178. DOI 10.1016/j.marpetgeo.2008.10.002

Ghienne, J.-F., Boumendjel, K., Paris, F., Videt, B., Racheboeuf, P. & Salem, H.A. 2007. The Cambrian–Ordovician succession in the Ougarta Range (western Algeria, North Africa) and interference of the Late Ordovician glaciation on the development of the Lower Palaeozoic transgression on northern Gondwana. *Bulletin of Geosciences 82*, 183–214. DOI 10.3140/bull.geosci.2007.03.183

Ghienne, J.-F., Monod, O., Kozlu, H. & Dean, W.T. 2010. Cambrian–Ordovician depositional sequences in the Middle East: A perspective from Turkey. *Earth-Science Reviews 101*, 101–146. DOI 10.1016/j.earscirev.2010.04.004

Ghienne, J.-F., Desrochers, A., Vandenbroucke, T.R.A., Achab, A., Asselin, E., Dabard, M.-P., Farley, C., Loi, A., Paris, F., Wickson, S. & Veizer, J. 2014. A Cenozoic-style scenario for the end-Ordovician glaciation. *Nature Communications 5*, 4485. DOI 10.1038/ncomms5485

Ghienne, J.-F., Abdallah, H., Deschamps, R., Guiraud, M., Gutiérrez-Marco, J., Konaté, M., Meinhold, G., Abderamane, M. & Rubino, J.-L. 2023. The Ordovician record of North and West Africa: unravellig sea-level variations, Gondwana tectonics, and the glacial impact. *Geological Society London, Special Publication 533*, 199–252. DOI 10.1144/SP533-2022-213

Gil-Ortiz, M., Mcdougall, N.D., Cabello, P., Marzo, M. & Ramos, E. 2019. Sedimentology of a "nonactualistic" Middle Ordovician tidal-influenced reservoir in the Murzuq Basin (Libya). *AAPG Bulletin 103*, 2219–2246. DOI 10.1306/02151918138

Gil-Ortiz, M., Mcdougall, N.D., Cabello, P., Marzo, M. & Ramos, E. 2022. Sedimentary architecture of a Middle Ordovician embayment in the Murzuq Basin (Libya). *Marine and Petroleum Geology 135*, 105339. DOI 10.1016/j.marpetgeo.2021.105339

Gomes Silva, M., Pacaud, M. & Wiel, F. 1963. Contribution à l'étude du Cambro-Ordovicien des chaines d'Ougarta (Sahara algérien). *Bulletin de la société géologique de France 7*, 134–141. DOI 10.2113/gssgfbull.S7-V.1.134

Gradstein, F., Ogg, J.G., Schmitz, M.D. & Ogg, G.M. 2012. *The Geologic Time Scale 2012.* 1175 pp. Elsevier.

Gutiérrez-Marco, J.C. & Vinn, O. 2018. Cornulitids (tubeworms) from the late Ordovician Hirnantia fauna of Morocco. *Journal of African Earth Sciences 137*, 61–68. DOI 10.1016/j.jafrearsci.2017.10.005

Hamdidouche, R. 2009. *Le bassin intra-cratonique de l'Ougarta (SW-Algérie): Évolution géodynamique au paléozoïque*. 175 pp. Ph.D. thesis, Université des Sciences et Technologie Houari Boumediene, Algiers, Algeria.

Harms, J.C., Southard, J.B., Spearing, D.R. & Walker, R.G. 1975. Depositional environments as interpreted from primary sedimentary structures and stratification sequences, *SEPM Short course number 2*, 1–161. DOI 10.2110/scn.75.01.0001

Hove, H.A.T & Smith, R.S. 1990. A re-description of *Ditrupa gracillima* Grube, 1878 (Polychaeta, Serpulidae) from the Indo-Pacific, with a discussion of the genus. *Records of the Australian Museum 42*, 101–118. DOI 10.3853/j.0067-1975.42.1990.108

Jelby, M.E., Grundvåg, S.A., Helland-Hansen, W., Olaussen, S. & Stemmerik, L. 2020. Tempestite facies variability and storm–depositional processes across a wide ramp: Towards a polygenetic model for hummocky cross–stratification. *Sedimentology 67*, 742–781. DOI 10.1111/sed.12671

Kidwell, S.M., Fürsich, F.T. & Aigner, T. 1986. Conceptual Framework for the analysis and classification of fossil concentration. *Palaios 1*, 228–238. DOI 10.2307/3514687

Kondo, Y., Abbott, S.T., Kitamura, A., Kamp, P.J.J., Naish, T.R., Kamataki, T. & Saul, G.S. 1998. The relationship between shellbed type and sequence architecture: examples from Japan and New Zealand. *Sedimentary Geology 122*, 109–127. DOI 10.1016/S0037-0738(98)00101-8

Lamali, A., Merabet, N., Henry, B., Maouche, S., Graine–Tazerout, K., Mekkaoui, A. & Ayache, M. 2013. Polyphased geodynamical evolution of the Ougarta (Algeria) magmatic complexes evidenced by paleomagnetic and AMS studies. *Tectonophysics 588*, 82–99. DOI 10.1016/j.tecto.2012.12.007

Legrand, P. 1966. Précisions biostratigraphiques sur l'Ordovicien inférieur et le Silurien des chaînes d'Ougarta (Sahara algérien). *Comptes Rendus Sommaires des Séances de Société Géologique de France 1966(7)*, 243–245.

Legrand, P. 1974. Essai sur la paléogéographie de l'Ordovicien du Sahara algérien. *Compagnie Française des Pétroles, Notes et Mémoires 11*, 121–138.

Legrand, P. 1985. Lower palaeozoic rocks of Algeria, 5–89. *In* Holland, C.H. (ed.) *Lower Palaeozoic of north-western and west-central Africa*. Wiley.

Legrand, P. 2003. Late Ordovician-early Silurian paleogeography of the Algerian Sahara. *Bulletin de la Société Géologique de France 174*, 19–32. DOI 10.2113/174.1.19

Legrand, P. & Bouterfa, B. 2021. The shaly-sandy Bou M'haoud Formation (Late Ordovician-pre-latest ordovician disconformity) at its type-locality and adjoining outcorps (Ougarta Range, Algerian Sahara). *Bulletin du Service Géologique de l'Algérie 30*, 51–112.

Li, C., Wang, P., Daidu, F., Bing, D. & Tiesong, L. 2000. Open-coast intertidal deposits and the preservation potential of individual laminae: a case study from east-central China. *Sedimentology 47*, 1039–1051. DOI 10.1046/j.1365-3091.2000.00338.x

Loi, A., Ghienne, J.F., Dabard, M.P., Paris, F., Botquelen, A., Christ, N., Elaouad-Debbaj, Z., Gorini, A., Vidal, M., Videt, B. & Destombes, J. 2010. The Late Ordovician glacio-eustatic record from a high-latitude storm-dominated shelf succession: The Bou Ingarf section (Anti-Atlas, Southern Morocc). *Palaeogeography Palaeoclimatology Palaeoecology 296*, 332–358. DOI 10.1016/j.palaeo.2010.01.018

Makhlouf, Y., Nedjari, A., Dahoumane, A., Nardin, E., Nohejlova, M. & Lefebvre, B. 2018. Palaeobiogeographic implications of the first report of the eocrinoid genus *Ascocystites* Barrande (Echinodermata, Blastozoa) in the Upper Ordovician of the Ougarta Range (Western Algeria). *Annales de Paléontologie 104*, 301–307. DOI /10.1016/j.annpal.2018.07.001

Marante, A. 2008. *Architecture et dynamique des systèmes sédimentaires silico-clastiques sur "la plate-forme géante" nord-gondwanienne. L'Ordovicien moyen de l'Anti-Atlas marocain*. 229 pp. Ph.D. thesis, Université Bordeaux 3, France.

Meddour, A. 2016. *Les séries de l'Ordovicien moyen et supérieur de l'Anti-Atlas oriental (Maroc)*. 298 pp. Ph.D. thesis, Université Bordeaux 3, France.

Mehadji, A.O., Tewfik Atif, K.F., Bouterfa, B., Nicollin, J.-P. & Besseghier, F.Z. 2011. Environnements sédimentaires de la Saoura-Ougarta (Sahara Nord-Ouest, Algérie) au Dévonien inférieur (Lochkovien supérieur pro parte -Emsien). *Geodiversitas 33*, 553–580. DOI 10.5252/g2011n4a2

Mekkaoui, A., Remaci-Bénaouda, N. & Graine-Tazerout, K. 2017. Mafic dikes at Kahel Tabelbela (Daoura, Ougarta Range, south-western Algeria): New insights into the petrology, geochemistry and mantle source characteristics. *Comptes Rendus Geoscience 349*, 202–211. DOI 10.1016/j.crte.2017.06.003

Melouah, O., López Steinmetz, R.L. & Ebong, E.D. 2021. Deep crustal architecture of the eastern limit of the West African Craton: Ougarta Range and Western Algerian Sahara. *Journal of African Earth Sciences 183*, 104321. DOI 10.1016/j.jafrearsci.2021.104321

Menchikoff, N. 1930. Recherches géologiques et morphologiques dans le Nord du Sahara occidental. *Revue de Géographie physique et de géologie dynamique 3*, 103–249.

Metatla, I. 2023. *Paléoenvironnements et dynamique sédimentaire des dépôts littoraux de l'Ordovicien de la Daoura, SW Algérie*. 208 pp. Ph.D. thesis, Université de Lille.

Michard, A., Driouch, Y., Kuiper, Y.D., Caby, R., Farah, A., Ouanaimi, H., Soulaimani, A., Chabou, M.C. & Saddiqi, O. 2023. The Variscan belts of North-West Africa: An African legacy to the Wilson Cycle concept. *Journal of African Earth Sciences 208*, 105042. DOI 10.1016/j.jafrearsci.2023.105042

Naimi, M.N., Bouterfa, B., Vinn, O. & Ghenne, R. 2023. Ichnological analysis of the Kheneg el Aatène Formation (Floian-Dapingian) at its type locality (Saoura Valley, Ougarta Range, Southwesten Algeria). *Historical Biology*, 1–14. DOI 10.1080/08912963.2023.2257728

Nedjari, A. & Ait Ouali, R. 2006. Le bassin d'Ougarta: Une mobilité permanente au paléozoïque. *Mémoire du Service Géologique National d'Algérie 13*, 23–40.

Passchier, S. & Kleinhans, M.G. 2005. Observations of sand waves, megaripples, and hummocks in the Dutch coastal area and their relation to currents and combined flow conditions: sand waves, megaripples and hummocks. *Journal of Geophysical Research 110*, F04S15. DOI 10.1029/2004JF000215

Perron, P., Guiraud, M., Vennin, E., Moretti, I., Portier, É., Le Pourhiet, L. & Konaté, M. 2018. Influence of basement heterogeneity on the architecture of low subsidence rate Paleozoic intracratonic basins (Reggane, Ahnet, Mouydir and Illizi basins, Hoggar Massif). *Solid Earth 9*, 1239–1275. DOI 10.5194/se-9-1239-2018

Plink-Björklund, P. 2008. Wave-to-tide process change in a Campanian Shoreline Complex, Chimney Rock Tongue, Wyoming/Utah, 265–291. *In* Hampson, G.J., Stell, R.J., Burgess, P.M. & Dalrymple, R.W. (eds) *Recent advances in Models of Siliciclastic Shallow-Marine Stratigraphy. SEPM Special publication 90*. DOI 10.2110/pec.08.90.0265

Poiré, D.G., Spalletti, L.A. & Valle, A.D. 2003. The Cambrian-Ordovician siliciclastic platform of the Balcarce Formation (Tandilia System, Argentina): Facies, trace fossils, palaeoenvironments and sequence stratigraphy. *Geologica Acta 1*, 41–60.

Popov, L.E., Legrand, P., Bouterfa, B. & Ghobadi Pour, M. 2019. Ordovician cold-water brachiopods from the Ougarta Mountain Range, Algerian Sahara. *Bulletin of Geoscience 94*, 41–70. DOI 10.3140/bull.geosci.1726

Poueyto, A. 1952. Rhyolites et grès d'Ougarta, 25–35. *In* Alimen, H. et al. (eds) *Les chaînes d'Ougarta et la Saoura. 19e Congrès Géologique Interne. Algérie 15*.

Reynaud, J.-Y. & Dalrymple, R.W. 2012. Shallow-Marine Tidal Deposits, 335–369. *In* Davis, R.A., Jr. & Dalrymple, R.W. (eds) *Principles of Tidal Sedimentology.* Springer, Dordrecht. DOI 10.1007/978-94-007-0123-6_13

Rossi, V.M. & Steel, R.J. 2016. The role of tidal, wave and river currents in the evolution of mixed-energy deltas: example from the Lajas Formation (Argentina). *Sedimentology 63*, 824–864. DOI 10.1111/sed.12240

Sabaou, N., Ait-Salem, H. & Zazoun, R.S. 2009. Chemostratigraphy, tectonic setting and provenance of the Cambro-Ordovician clastic deposits of the subsurface Algerian Sahara. *Journal of African Earth Sciences 55*, 158–174. DOI 10.1016/j.jafrearsci.2009.04.006

Shchepetkina, A., Gingras, M.K., Mángano, M.G. & Buatois, L.A. 2019. Fluvio-tidal transition zone: Terminology, sedimentological and ichnological characteristics, and significance. *Earth-Science Reviews 192*, 214–235. DOI 10.1016/j.earscirev.2019.03.001

Sherman, D.J. & Greenwood, B. 1989. Hummocky cross-stratification and post-vortex ripples: length scales and hydraulic analysis. *Sedimentology 36*, 981–986. DOI 10.1111/j.1365-3091.1989.tb01535.x

Stride, A.H. 1982. Offshore tidal deposits: sand sheet and sand bank facies, 95–125. *In* Stride, A.H. (ed.) *Offshore Tidal Sands: Processes and deposits*. Springer Netherlands, Dordrecht. DOI 10.1007/978-94-009-5726-8_5

Vakarelov, B.K., Ainsworth, R.B. & Maceachern, J.A. 2012. Recognition of wave-dominated, tide-influenced shoreline systems in the rock record: Variations from a microtidal shoreline model. *Sedimentary Geology 279*, 23–41. DOI 10.1016/j.sedgeo.2011.03.004

Vaucher, R., Martin, E.L.O., Hormière, H. & Pittet, B. 2016. A genetic link between Konzentrat- and Konservat-Lagerstatten in the Fezouata Shale (Lower Ordovician, Morocco). *Palaeogeography Palaeoclimatology Palaeoecology 460*, 24–34. DOI 10.1016/j.palaeo.2016.05.020

Vaucher, R., Hormière, H., H., Pittet, B., Martin, E.L.O. & Lefebvre, B. 2017. A wave-dominated, Tide-modulated model for the Lower Ordovician of the Anti-Atlas, Morocco. *Sedimentology 64*, 777–807. DOI 10.1111/sed.12327

Vinn, O. 2010. Adaptive strategies in the evolution of encrusting tentaculitoid tubeworms. *Palaeogeography Palaeoclimatology Palaeoecology 292*, 211–221. DOI 10.1016/j.palaeo.2010.03.046

Vinn, O. & Zatoń, M. 2012. Phenetic phylogenetics of tentaculitoids – extinct problematic calcareous tube-forming organisms. *GFF 134*, 145–156. DOI 10.1080/11035897.2012.669788

Walker, R.G. 1984. Shelf and shallow marine sands, 141–169. *In* Walker, R.G. (ed.) *Facies models – 1st ed*. Geological Association of Canada.

Walker, R.G. 1992. Wave-and strom-dominated shallow marine systems, 219–238. *In* Walker, R.G. & James, N.P. (eds) *Facies Models-Response to sea level change*. Geological Association of Canada.

Yang, B.C., Dalrymple, R.W. & Chun, S. 2005. Sedimentation on a wave-dominated, open-coast tidal flat, south-western Korea: summer tidal flat- winter shoreface. *Sedimentology 52*, 235–252. DOI 10.1111/j.1365-3091.2004.00692.x

Yang, B.C., Dalrymple, R.W. & Chun, S. 2006. The significance of hummocky cross-stratification (HCS) wavelenghs: Evidence from an open-coast tidal flat, South Korea. *Journal of Sedimentary Research 76*, 2–8. DOI 10.2110/jsr.2006.01

Zecchin, M. & Catuneanu, O. 2013. High-resolution sequence stratigraphy of clastic shelves I: Units and bounding surfaces. *Marine and Petroleum Geology 39*, 1–25. DOI 10.1016/j.marpetgeo.2012.08.015

Ziegler, P.A., Cloetingh, S. & Van Wees, J.-D. 1995. Dynamics of intra-plate compressional deformation: the Alpine foreland and other examples. *Tectonophysics 252*, 7–59.